https://doi.org/10.5194/egusphere-2026-6709
Preprint. Discussion started: 16 November 2026
© Author(s) 2026. CC BY 4.0 License.

Ecosystem CO_2 flux of a lake habitat with submerged vegetation

Lei Jia[1, 2], Mi Zhang[1], Wei Xiao[1, 3], Yini Pu[4], Zhen Zhang[5], Pei Ge[2], Fuyu Yang[2], Hengxin Bao[6], Yang He[7], and Xuhui Lee[8]

[1]Yale-NUIST Center on Atmospheric Environment, Collaborative Innovation Center on Forecast and Evaluation of Meteorological Disasters, Nanjing University of Information Science & Technology, Nanjing, 210044, China
[2]Jiangsu Provincial Meteorological Data Center, Nanjing, 211000, China
[3]State Key laboratory of Climate System Prediction and Risk Management, Nanjing University of Information Science & Technology, Nanjing, 210044, China
[4]Office of Development Planning and Discipline Construction, Chengdu University of Technology, Chengdu, 610059, China
[5]Nanjing Jiangning District Meteorological Bureau, Nanjing, 211100, China
[6]Hebei Xiong'an New Area Meteorological Bureau, Xiong'an New Area, 071000, China
[7]Liaoning Agricultural Meteorology and Satellite Remote Sensing Center, Shenyang, 110166, China
[8]School of the Environment, Yale University, New Haven, 06511, USA

Correspondence to: Mi Zhang (zhangm.80@nuist.edu.cn), Xuhui Lee (xuhui.lee@yale.edu)

Abstract. Submerged aquatic vegetation (SAV) can grow rapidly in shallow lakes, but the extent to which its growth is supported by atmospheric CO_2 remains poorly understood. In this study, the air-water CO_2 flux was measured with a closed-path eddy covariance system in a SAV zone of Lake Taihu, China, from July 2020 to December 2023. Satellite-derived vegetation indices and dissolved CO_2 measurements were used to investigate the influence of vegetation seasonality and water-column CO_2 storage on the flux. The habitat was a net CO_2 source during the winter and spring and a sink in the late summer to early autumn. The annual net flux was positive, indicating emission, at 45 and 89 g CO_2 m^{-2} yr^{-1} in 2022 and 2023, respectively, indicating that uptake during peak SAV coverage was insufficient to offset emission in the other months. At the monthly scale, the normalized difference vegetation index explained 45% of the observed flux variability. At the half-hourly scale, the flux showed no clear dependence on solar radiation or water temperature. The water-column storage flux had a greater diurnal amplitude than the air–water flux measured by eddy covariance, suggesting that the dissolved CO_2 pool buffered the exchange between underwater vegetation and the atmosphere. Nighttime CO_2 uptake and declining dissolved CO_2 concentrations during the first half of the night provided some evidence for Crassulacean Acid

https://doi.org/10.5194/egusphere-2026-6709
Preprint. Discussion started: 16 November 2026
© Author(s) 2026. CC BY 4.0 License.

Metabolism. These observations show that water-column carbon storage plays an important role in supporting SAV CO_2 uptake and weakens its temporal coupling with atmospheric CO_2 exchange.

1 Introduction

Submerged aquatic vegetation (SAV) – plants rooted in the soil and growing under water – is an integral component of inland waters and coastal marine ecosystems. Having low C:N ratios, SAV biomass is an important source of food for fish and birds (Bakker et al., 2016). SAV canopies provide refuge against predation and enhance the richness of invertebrate communities (Scheffer, 2004). The presence of plants underwater suppresses the transfer of momentum from the overlying atmosphere to the lake (Xiao et al., 2013) and turbulent motion in the water column (Pujol et al., 2010), serving along with the root system to stabilize the sediment against erosion and resuspension in high wind events. Reduction in sediment resuspension lowers the risk of reactivation of P and N bounded in the soil. In open waters without SAV protection, strong winds are known to enhance the transfer of P and N from the sediment to the water column, triggering algal blooms (Wu et al., 2015; Zhu et al., 2015). Water is less turbid if it is inhabited by SAV (Scheffer, 2004), and as a result, the aesthetic value of the lake is improved and the lake water is more suitable for human consumption.

The growth of SAV exhibits a seasonal pattern regulated by temperature and light availability. Typically, SAV begins to sprout in the early spring, reaches peak biomass in the midsummer, and gradually declines in the autumn as light intensity and temperature decrease (Schloesser et al., 1985; Wu et al., 2021; Mo et al., 2026). Their belowground structures, including rhizomes and tubers, enable overwintering and regrowth in the following spring (Adamec, 2018; Luo et al., 2016). Seasonal variations in canopy height and leaf area affect underwater light distribution and photosynthetic capacity, leading to large seasonal changes in primary productivity and carbon assimilation (Ward et al., 2022; Pedersen et al., 2013; Kelly et al., 1983).

It is generally thought that the growth of SAV is limited by carbon availability (Maberly and Madsen, 2002; Baattrup-Pedersen et al., 2013). A vast pool of carbon dioxide exists in the atmosphere, but

https://doi.org/10.5194/egusphere-2026-6709
Preprint. Discussion started: 16 November 2026
© Author(s) 2026. CC BY 4.0 License.

atmospheric CO_2 must first pass through the thin interfacial layer at the water surface, which is a diffusion barrier, before it can be utilized for photosynthesis. That CO_2 diffuses 10, 000 times slower in water than in air further hampers macrophyte growth (Pedersen et al., 2013). Paradoxically, explosive growth of SAV has been reported for shallow lakes (Hilt et al., 2006; Verhofstad and Bakker, 2019). At Lake Taihu, we observed instances of such growth between site visits: no vegetation was visible from our instrument platform on a site visit, but on the next site visit a month later the water surrounding the platform would be clogged by dense meshes of biomass. Such growth is a concern for water resource management because it is detrimental to recreation use and can block navigation routes (Verhofstad and Bakker, 2019). Another concern is that excessive accumulation of organic matter in the sediment can turn a lake into marshland (Carpenter, 1981). One hypothesis is that diffusion is not a limitation at times of rapid growth, so atmospheric CO_2 can fuel such growth. An alternative hypothesis is that the growth is supported by DIC in the water column. Given the shallowness of these lakes, this would result in substantial reduction in, if not complete depletion of DIC, or else it would require that the lake water column maintains high enough capacity to buffer the DIC changes (Andersen et al., 2019; Sand-Jensen et al., 2019). We suggest that one way to determine which of the two hypotheses is valid is via direct observation of the water-air CO_2 flux.

To compensate for the carbon limitation, many SAV species have developed Crassulacean Acid Metabolism (CAM) mechanism (Keeley, 1998), whereby CO_2 is fixed by PEPC into malic acid at night and in the subsequent daylight period the acid is decarboxylated to yield CO_2 for fixation by Rubisco. CAM allows the plants to extend carbon uptake to the full diurnal cycle (Keeley and Bowes, 1982). So far, evidence for CAM has been provided by destructive sampling of SAV plant leaves and analysis of changes of malic acid concentration in the leaf samples over the diurnal cycle (Klavsen et al., 2011). It is difficult to scale these destructive leaf-scale measurements to the whole intact ecosystem because the ratio of acid accumulation to carbon fixation varies in field conditions (Nobel and Hartsock, 1983). In-situ measurement of oxygen accumulation in the water column has been widely used to quantify photosynthesis of phytoplankton, on the basis of stoichiometry of carbon assimilation (Winslow et al., 2016). This stoichiometry method is not applicable to SAV because some oxygen released during

https://doi.org/10.5194/egusphere-2026-6709
Preprint. Discussion started: 16 November 2026
© Author(s) 2026. CC BY 4.0 License.

photosynthesis is retained in the plant tissues and is later consumed by respiration and because oxygen can escape the water column as bubbles (Wetzel, 2001; Shikhani et al., 2024). In a land ecosystem that utilizes CAM for growth, its net ecosystem exchange is often negative at night, indicating CO_2 uptake from the atmosphere (Owen et al., 2016). If CAM is an important photosynthetic pathway for SAV, it is reasonable to expect that the lake would also be a sink of atmospheric CO_2 at night.

Related to the issue of diffusion limitation is seasonal variation in water depth. Lakes inhabited by SAV are shallow. Their depth can fluctuate at monthly to seasonal timescale due to variations in precipitation (Zhu et al., 2019; Wu and Liu, 2017). Shallower waters enhance light penetration and turbulent mixing, facilitating CO_2 uptake (Ersoy et al., 2020; G.-Tóth et al., 2011). Additionally, reduced water depth brings plant canopies closer to the surface, shortening the diffusion path and diminishing the buffering capacity of the overlying water column. This may decrease the lag between the CO_2 flux across the water-air interface and photosynthetic activity within the canopy.

Although the ecological significance of SAV has been widely recognized, direct and continuous observations of the CO_2 flux in SAV habitats remain scarce. We are aware of only one such study in coastal lagoons (Tokoro et al., 2014), but no studies have reported continuous CO_2 flux observation in SAV habitats in inland waters. The eddy-covariance (EC) technique is a direct method of measuring CO_2 exchange between ecosystems and the atmosphere, capturing high-frequency variations jointly driven by biological processes and environmental forcing. The strong physical and chemical buffering within the water column may mask the temporal coupling between vegetation activity and air–water gas exchange, highlighting the importance of high-frequency flux measurements (Podgrajsek et al., 2015; Golub et al., 2023). Its non-intrusive nature and ability to integrate fluxes at the ecosystem spatial scale are two other advantages over destructive sampling or laboratory experiments for assessing carbon dynamics in complex aquatic environments.

This study aims to address this knowledge gap using multi-year (July 2020 to December 2023) EC observations at Lake Taihu, in a lake zone where SAV is abundant. Lake Taihu is a large and shallow

https://doi.org/10.5194/egusphere-2026-6709
Preprint. Discussion started: 16 November 2026
© Author(s) 2026. CC BY 4.0 License.

freshwater lake in Eastern China. We seek to (1) quantify the influence of diurnally varying solar radiation on CO_2 flux dynamics, (2) investigate whether the EC-observed above-water CO_2 flux captures the seasonal growth and photosynthetic activity of SAV, (3) determine whether CAM for carbon capture is strong enough to generate CO_2 uptake from the atmosphere at night, and (4) examine if water depth and other key abiotic factors control flux variability across hourly, monthly, and interannual scales.

2 Materials and Methods

2.1 Site

The study was conducted at the Bifenggang (BFG) site, located in the eastern part of Lake Taihu (31.36°N, 120.37°E), a large, shallow, subtropical lake in the Yangtze River Delta region of eastern China (Fig. 1). Lake Taihu has an average depth of 1.9 m and a surface area of 2,400 km². The BFG site is characterized by extensive submerged macrophyte coverage, dominated by *Hydrilla verticillata* and *Potamogeton malaianus*, which form dense underwater meadows during the growing season (Zhao, 2017; Dong et al., 2017). The site is part of the Lake Taihu eddy flux mesonet program (Lee et al., 2014).

Field photographs collected from June 2019 to May 2020 provided visual documentation of the aquatic vegetation conditions around the site (Fig. S1 and S2). From June to November 2019, extensive patches of vegetation were present near the water surface. In December 2019, vegetation cover decreased substantially. January to April 2020 was a period of open water. Sparse vegetation reappeared in May 2020, indicating the beginning of a new growing season.

2.2 Micrometeorological observation

A closed-path eddy covariance (CPEC) system has been continuously operated at the site since July 2020. This study is based on the data collected between July 2020 and December 2023. The system consisted of a closed-path CO_2/H_2O gas analyzer (model EC155, Campbell Scientific, Logan, Utah, USA), a three-dimensional sonic anemometer (model CSAT3, Campbell Scientific), a datalogger (model CR6, Campbell Scientific), a sampling pump, and a three-valve module for automatic zero and span calibrations. The system was mounted at a height of ~8.5 m above the water surface. Air was drawn through a sampling

https://doi.org/10.5194/egusphere-2026-6709
Preprint. Discussion started: 16 November 2026
© Author(s) 2026. CC BY 4.0 License.

inlet into the EC155 analyzer for measurement of CO_2 and H_2O concentrations. The inlet was configured with a vortex intake designed to minimize the entry of dust and aerosol particles into the optical cell. The sampling tube was a stainless-steel tube with a length of 64.5 cm and an inner diameter of 2.16 mm. The sample cell volume of the analyzer was 5.9 mL, the sampling flow rate was 7 L min^{-1}, and the sampling frequency was 10 Hz.

To ensure data quality, the EC155 analyzer was subject to automatic zero and CO_2 span calibrations once every 3 d. The span calibration was performed using a standard CO_2 gas with a mixing ratio of 400 ppm, provided by the National Institute of Metrology, China.

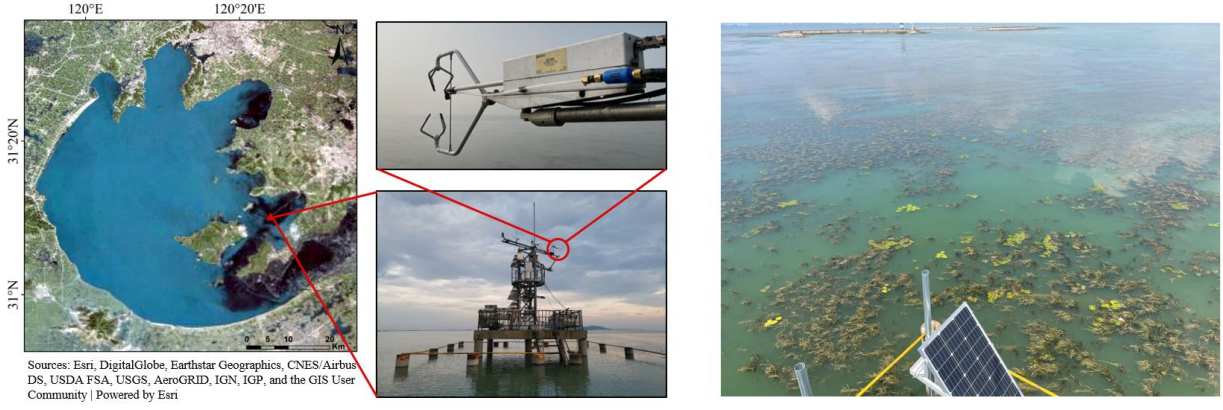


Figure 1. Measurement site and instrumentation. The left panel shows the location of the observation platform on a satellite basemap from Esri World Imagery Wayback (version: 11 June 2014; imagery and map data sources: Esri, DigitalGlobe, Earthstar Geographics, CNES/Airbus DS, USDA FSA, USGS, AeroGRID, IGN, IGP, and the GIS User Community; powered by Esri). The middle panels show the measurement platform and the closed-path eddy covariance system. The right panel is a photo taken on 3 August 2022, showing dense submerged vegetation near the platform. All three photographs were taken by the first author (Lei Jia).

An open-path eddy-covariance (OPEC) system was operated in parallel with the CPEC. It consisted of an open-path CO_2/H_2O gas analyzer (model EC150, Campbell Scientific) and a three-dimensional sonic anemometer (model CSAT3A, Campbell Scientific). The system measured CO_2 and H_2O densities, three-

https://doi.org/10.5194/egusphere-2026-6709
Preprint. Discussion started: 16 November 2026
© Author(s) 2026. CC BY 4.0 License.

dimensional wind components, and sonic temperature at a sampling frequency of 10 Hz. The OPEC measurements were subsequently used to correct the CPEC errors caused by aerosol interference (Section 2.5).

Supporting meteorological variables included the four components of the radiation balance, measured with a CNR4 net radiometer (Kipp & Zonen B.V., Delft, the Netherlands), air temperature and relative humidity measured with an HMP155A sensor (Vaisala, Helsinki, Finland), and wind speed and direction measured with an anemometer (Model 03002, R. M. Young Company, Traverse City, MI, USA). Water temperature profiles were measured using temperature probes (Model 109-L, Campbell Scientific) at depths of 0.2, 0.5, 1.0, 1.5, and 2.0 m below the water surface. All measurements were recorded as 30-min averages.

2.3 Observation of CO_2 concentration in water

The CO_2 concentration in the water was measured using an equilibration device constructed following the designs of Aho et al. (2021) and McGillis et al. (2001), from May 2019 to December 2020. The device consisted of a U-shaped PVC tube (inner diameter 5 cm) with a sealed long arm and an open short arm. Water was pumped at a depth of 20 cm from the lake using a submersible pump (Mini Typhoon, Proactive Environmental Products International LLC, Bradenton, FL, USA) and delivered to the top of the long arm of the U-tube, where it was dispersed through a nozzle into small droplets. This delivery method increased the gas-liquid contact area, facilitating the CO_2 exchange between the dissolved phase and the headspace air. The system reached a stable gas-liquid equilibrium after about 4 min. The system was switched on at the start of the hour for 5 min. Data collected from the last 1 min was used in the subsequent analysis. The CO_2 concentration in the headspace was measured using a non-dispersive infrared CO_2 analyzer (LI-840, LI-COR Inc., Lincoln, NE, USA), and the corresponding concentration of CO_2 dissolved in the water was calculated using the gas-liquid equilibrium principle.

https://doi.org/10.5194/egusphere-2026-6709
Preprint. Discussion started: 16 November 2026
© Author(s) 2026. CC BY 4.0 License.

2.4 NDVI calculation

The normalized difference vegetation index (NDVI) was used to characterize the growth status and seasonal dynamics of SAV. The area encompassing 90% of the cumulative turbulent flux contribution for each month was determined using the flux footprint model (Kljun et al., 2015) and defined as the study area for that month. Sentinel-2 Level-2A surface reflectance data were obtained for each monthly study area, and cloud- and cloud-shadow-contaminated pixels were masked out using the scene classification layer. NDVI was calculated for each scene at a spatial resolution of 10 m. Monthly NDVI composites were generated by taking the median of all valid NDVI observations at each pixel within each month. Monthly mean NDVI was then obtained by spatially averaging all valid pixels in each monthly composite within the corresponding study area.

To minimize the influence of open water on the remote sensing signal, a 500 m × 500 m open-water area near the PTS eddy-covariance site at the center of the lake (Lee et al., 2014) was selected as reference. This area contained no submerged macrophytes, and its NDVI represented the background signal of the open water surface. NDVI for the reference area was processed using the same cloud masking, monthly compositing, and spatial averaging procedures as those applied to the BFG study area. Fig. S3 presents the NDVI observed at BFG and PTS. In the following, we used the NDVI difference between the BFG site and the PTS reference area, denoted as ΔNDVI, to describe vegetation seasonality.

2.5 Data processing

The CO_2 flux measured with the CPEC system were calculated online using the EasyFlux DL CR6 CP program embedded in the CR6 data logger for the CPEC system. The CO_2 flux measured with the OPEC system was calculated offline using EddyPro software (LI-COR, Lincoln, NE, USA). High-frequency measurements of three-dimensional wind velocity and mole fractions of CO_2 and H_2O were screened using instrument diagnostic codes and signal strength. Then, the covariances between the wind components fluctuations and mole fraction of CO_2 were calculated over 30-min averaging intervals. The raw covariances were subsequently subject to double coordinate rotation (Wilczak et al., 2001), optimization of the time lag between the gas-concentration and vertical-wind-velocity signals (Horst and

https://doi.org/10.5194/egusphere-2026-6709
Preprint. Discussion started: 16 November 2026
© Author(s) 2026. CC BY 4.0 License.

Lenschow, 2009; Foken et al., 2012), the Webb–Pearman–Leuning correction for air-density fluctuations (Webb et al., 1980), as well as frequency response corrections for sensor spacing and sampling tube attenuation (Moncrieff et al., 1997).

We made an additional correction to remove errors caused by aerosol contamination. In an earlier study, we reported that broad-band analyzers used for open-path eddy covariance are interfered by aerosols in their optical path (L. Jia et al., 2024). Although a vortex filter was installed at the inlet of the analyzer of our CPEC system, some small aerosol particles could still enter the sampling line and interfere with the CO_2 signal, causing a negative bias in the measured flux. To remove this bias error, we applied the post-processing correction method proposed by L. Jia et al. (2024) to the CPEC dataset.

Let F_C be the true flux, F_{C_CP} be the CO_2 flux measured with the CPEC system, and F_{C_OP} be the flux measured simultaneously with the OPEC system (Fig. 2a). Following L. Jia et al. (2024), the difference between the observed flux and the true flux can be expressed as a linear function of the covariance between the optical signal strength and the vertical wind velocity:

$$F_{C_OP} - F_C = k(\overline{w's_o'}) \quad (1)$$

$$F_{C_CP} - F_C = k(\overline{w's_c'}) \quad (2)$$

where s_C and s_O denote the optical signal strengths measured by the CPEC and OPEC systems, respectively, and k is an empirical correction coefficient. Solving k from Equations (1) and (2), we obtain

$$k = \frac{F_{C_OP} - F_{C_CP}}{(\overline{w's_o'}) - (\overline{w's_c'})} \quad (3)$$

The corrected or true flux was obtained from

$$F_C = F_{C_CP} - k(\overline{w's_c'}) \quad (4)$$

Coefficient k was determined with a linear regression method. An example is given in Fig. 2. In this example, half-hourly observations during DOY 193 to 203 in 2023 were used to determine a diurnal

https://doi.org/10.5194/egusphere-2026-6709
Preprint. Discussion started: 16 November 2026
© Author(s) 2026. CC BY 4.0 License.

composite ΔFc (= $F_{C_OP} - F_{C_CP}$) and ΔCOV (= $(\overline{w's_o'}) - (\overline{w's_c'})$), yielding a total of 48 datapoints (one for each 30-min period). A clear linear relationship was observed between ΔF_C and ΔCOV, with a slope or k of 26388 μmol m^{-3} (Fig. 2b). This correction removed some anomalously negative nighttime CO_2 fluxes in the time series (Fig. 2c). The diurnal composite of the corrected flux for this time period, which was in the middle of the growing season, becomes well-behaved (Fig. 2d), showing positive values at night (flux from water to air) and negative values at midday (flux from air to water).

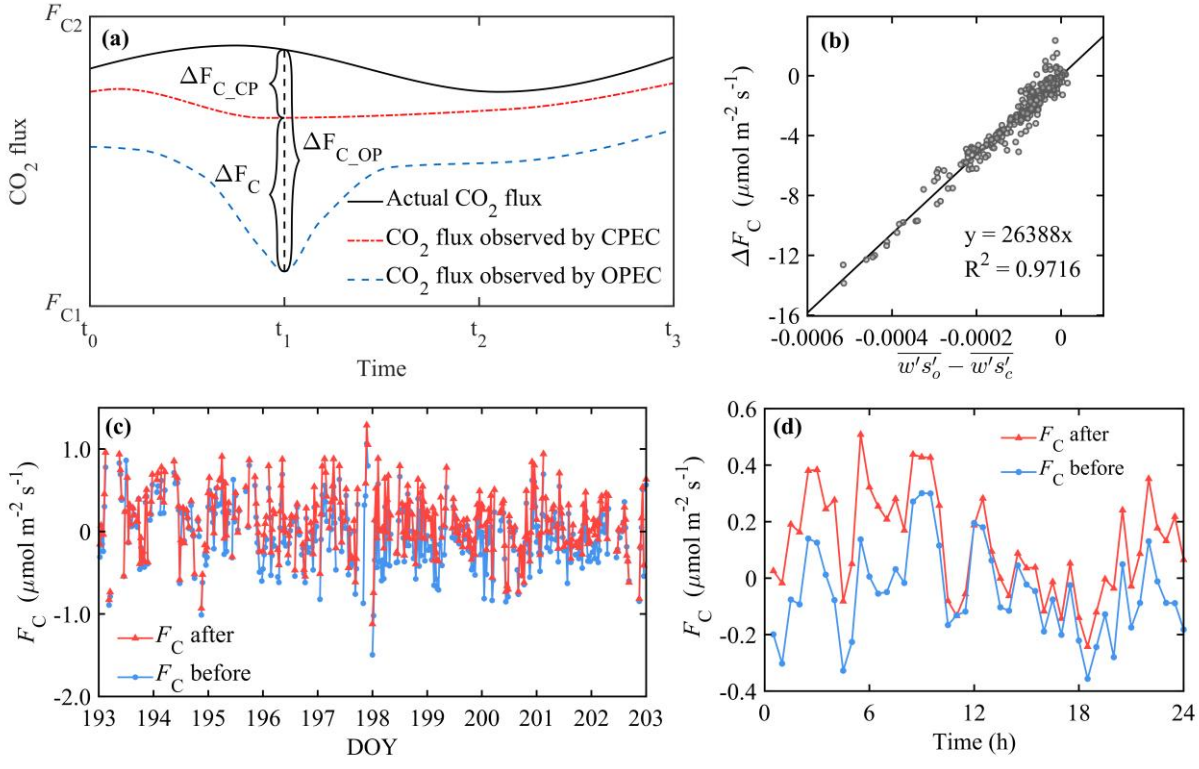


Figure 2. A schematic illustrating the procedure for correcting the aerosol interference with the CPEC CO_2 flux. (a) Conceptual representation of the actual and the observed flux. (b) Relationship between the difference in CO_2 flux observed with OPEC and CPEC (ΔF_C) and the corresponding difference in the covariance of vertical velocity and signal strength. (c) Half-hourly flux time series before and after correction. (d) Mean diurnal variations in the flux before and after correction.

https://doi.org/10.5194/egusphere-2026-6709
Preprint. Discussion started: 16 November 2026
© Author(s) 2026. CC BY 4.0 License.

In the results presented below, k was computed on a monthly basis to account for potential seasonal variations in aerosol physical and chemical properties. The k value ranges from 10993 (July 2020) to 38933 (May 2021).

We screened the nighttime CO_2 flux using a friction velocity (u_*) threshold to reduce errors under weak turbulence. Nighttime periods were identified based on downward shortwave radiation (DR), with half-hourly observations characterized by DR < 10 W m^{-2} classified as nighttime. A critical u_*threshold of 0.085 m s^{-1} was determined using the moving point test based on the relationship between the nighttime CO_2 flux and friction velocity. Nighttime observations with $u_* < 0.085$ m s^{-1} were excluded, and the remaining data were used for subsequent CO_2 flux analyses. After the u_* screening, valid half-hourly flux observations accounted for 57.3% of the total expected records.

Daily mean CO_2 fluxes were calculated only for days when more than 50% of the half-hourly CO_2 flux observations were valid. For days meeting this criterion, the daily mean CO_2 flux was calculated as the arithmetic mean of all available valid half-hourly observations within that day. Relationships between daily mean CO_2 fluxes and environmental variables were analysed using valid observations only, without gap filling.

Monthly mean CO_2 fluxes were calculated from the monthly averaged diurnal cycles. For each month, the mean flux for each half-hour interval was calculated using all available observations within that time window, resulting in a representative monthly diurnal cycle. The monthly mean CO_2 flux was subsequently calculated as the arithmetic mean of the 48 half-hourly values. Because no valid CO_2 fluxes were available for the entire month of February 2022, the monthly mean flux for this month was obtained through linear interpolation between the adjacent months.

https://doi.org/10.5194/egusphere-2026-6709
Preprint. Discussion started: 16 November 2026
© Author(s) 2026. CC BY 4.0 License.

3 Results

3.1 Environmental conditions

Over the study period, water depth varied from 2.9 to 4.8 m (Fig. 3). The highest value (4.8 m) occurred on 23 July 2020 (DOY 205) near the beginning of the experiment. It declined to about 3.0 m by the end of 2020. A secondary peak of 4.2 m occurred on 1 August (DOY 213) in 2021, after which it gradually decreased to 3.0 m at the end of the year. Water depth was relatively stable in 2022, fluctuating between 3.0 and 3.6 m. In 2023, water depth displayed two distinct rises during the middle and later parts of the year, with peaks of 3.7 m on 23 July (DOY 204) and 23 September (DOY 266), followed by subsequent declines.

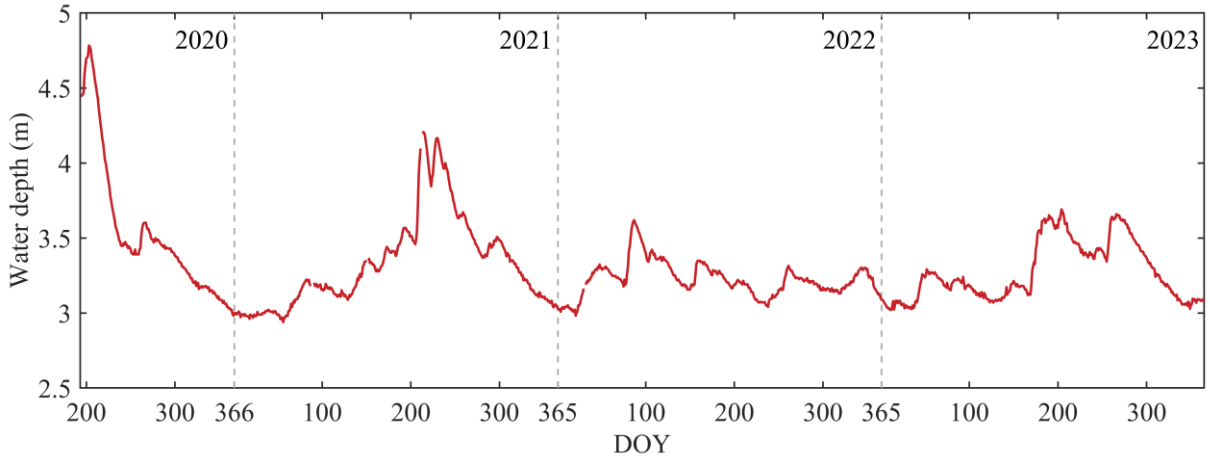


Figure 3. Daily water depth at the BFG flux observation site.

Fig. S4 shows the diurnal composites of four microclimate variables for each month. In every month, downward shortwave radiation (DR) increased during the morning, peaked around noon, and decreased in the afternoon. The noon maximum increased from 386.7 W m^{-2} in January to 704.9 W m^{-2} in August, and the duration of daylight extended from approximately 10 h in January to 14 h from May to July. Air temperature (Ta) and water temperature (Tw) at the depth of 20 cm increased progressively from January to August and then declined with time afterwards. The mean diurnal range of Ta was 4.7 °C in April and 2.6 °C in December, and that of Tw was 2.7 in August and 1.1 °C in December. The daily maximum of

https://doi.org/10.5194/egusphere-2026-6709
Preprint. Discussion started: 16 November 2026
© Author(s) 2026. CC BY 4.0 License.

Tw occurred approximately 1 h later than that of Ta and about 3.5 h later than that of DR. Wind speed varied within the range of 3.48–5.59 m s^{-1}. In most months (February to November), wind speed remained low during the night and early morning, increased gradually during the day, reached higher values at noon, and then decreased again with time. Seasonally, wind speed was higher in the summer than in the winter.

The vertical water temperature gradient in Lake Taihu showed marked seasonal variations (Fig. 4). Diurnal temperature variation was mainly confined to the surface water to a depth of about 20 cm and was more pronounced during the warm season than in the cold season. In the winter (December–February), a nighttime unstable stratification was observed, with surface water temperatures lower than bottom temperatures by 0.7 to 1.1 °C. In the spring (March–May), stable thermal stratification developed in the afternoon (between 13:00 and 18:00) in response to warming by solar radiation, with daytime surface-to-bottom temperature differences of approximately 1.3 to 2.8 °C. In the spring, the nighttime unstable stratification disappeared, and surface water was 0.2 to 0.9 °C warmer than bottom water at night. In the summer (June–August), stable thermal stratification was strongest, with the maximum daytime surface-to-bottom temperature difference of 2.4 to 3.0 °C (observed at ~15:30) and nighttime surface-to-bottom difference of 0.9 to 1.2 °C (observed at ~6:00). In the autumn (September–November), the maximum daytime surface-to-bottom thermal difference declined to 1.3 to 2.3 °C, indicating weakening of stable thermal stratification. Nighttime surface water temperatures remained higher than bottom water temperatures in September but were lower in October and November. The nighttime surface-to-bottom temperature difference reached −0.51 °C at 06:00 in November, indicating that unstable thermal stratification had returned.

https://doi.org/10.5194/egusphere-2026-6709
Preprint. Discussion started: 16 November 2026
© Author(s) 2026. CC BY 4.0 License.

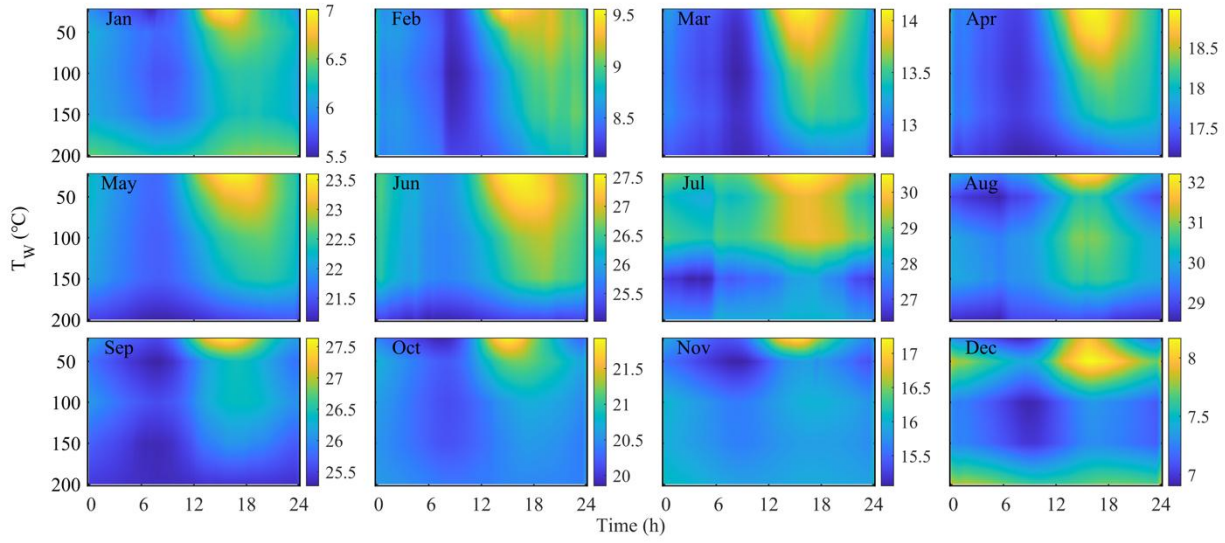


Figure 4. Monthly mean diurnal contour plots of water temperature. Temperature unit is °C.

NDVI exhibited seasonal and interannual variability (Fig. 5). From November to the following April, SAV was absent, and accordingly ΔNDVI remained close to zero. The period from May to September represented the growth phase, with ΔNDVI reaching its maximum around September. The seasonal signal was weakest in 2020, when ΔNDVI ranged from -0.136 in February to 0.082 in October. A more distinct seasonal cycle occurred in 2021, with ΔNDVI increasing from 0.017 in May to a maximum of 0.384 in September before declining to 0.004 in December. In 2022, the highest value was 0.234 in August, followed by a gradual decrease to 0.068 in December. The strongest seasonal ΔNDVI signal occurred in 2023, when ΔNDVI increased rapidly from 0.155 in May to a maximum of 0.552 in September and subsequently declined to -0.013 in December.

https://doi.org/10.5194/egusphere-2026-6709
Preprint. Discussion started: 16 November 2026
© Author(s) 2026. CC BY 4.0 License.

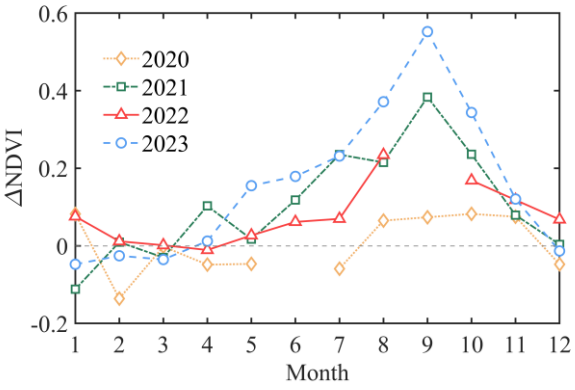


Figure 5. Seasonal variations in baseline-corrected NDVI (ΔNDVI) at the BFG site.

In the following, we divide the year into four growth periods: February to April (ΔNDVI near zero, SAV absent), May to July (SAV growth), August to October (peak SAV coverage), and November to January (senescence).

3.2 Time variations of CO_2 flux

Fig. 6 shows the monthly flux diurnal composites. The diurnal variation of F_C was most pronounced from August to October. During this period, the CO_2 flux showed weak emission (positive values) at night and shifted to uptake (negative values) after noon, with the maximum uptake in the later afternoon. The diurnal variation was weak in the other months.

https://doi.org/10.5194/egusphere-2026-6709
Preprint. Discussion started: 16 November 2026
© Author(s) 2026. CC BY 4.0 License.

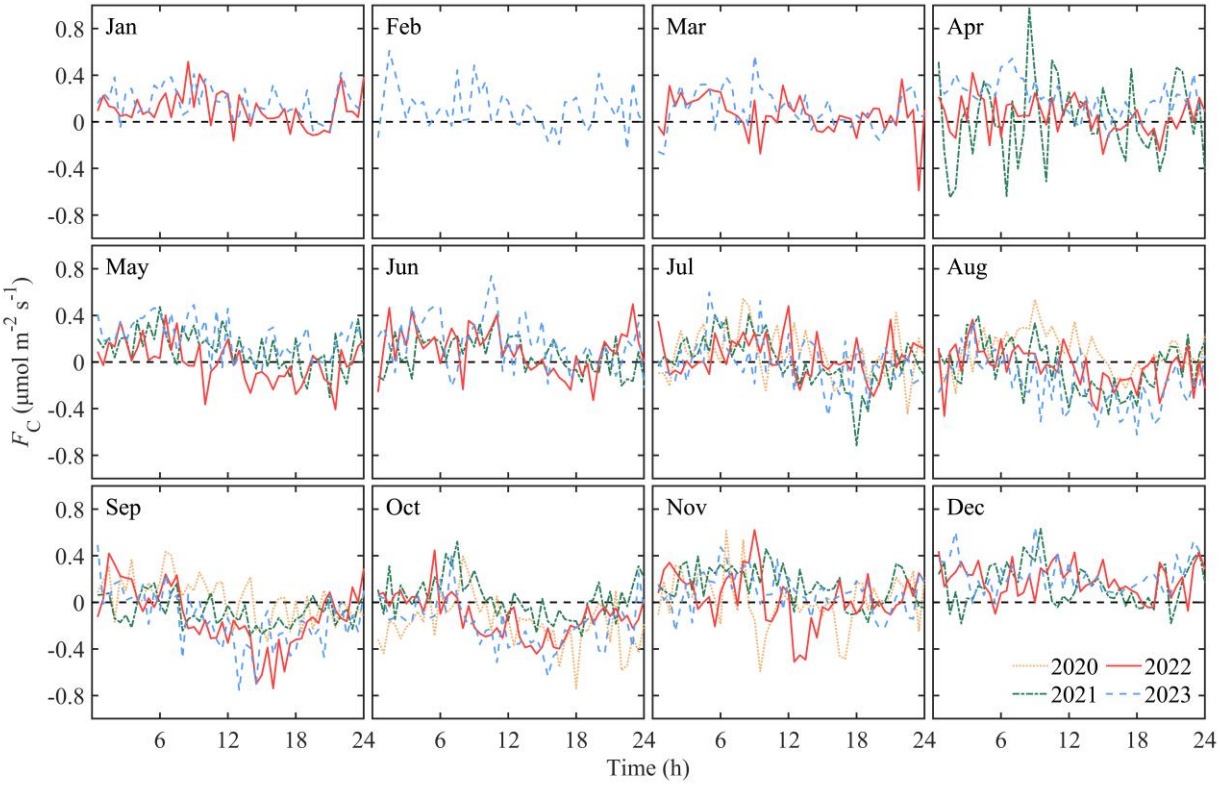


Figure 6. Diurnal CO_2 flux composite by month.

The CO_2 flux was not in phase with solar radiation. To quantify this phase shift, Fig. 7 compares the flux and the solar radiation diurnal composites averaged over each of the four growth periods. From February to April, SAV had not yet emerged, and the lake remained in a CO_2 emission state for most of the day, except for a brief period (from 15:00 to 16:30) showing weak CO_2 uptake. The composite CO_2 flux ranged from -0.087 to 0.352 μmol m^{-2} s^{-1}. From May to July, the composite flux ranged from -0.134 μmol m^{-2} s^{-1} (17:30) to 0.289 μmol m^{-2} s^{-1} (05:30). From August to October, when SAV was most abundant, the diurnal variation in F_C was pronounced with a range of 0.146 μmol m^{-2} s^{-1} at 07:00 to -0.342 μmol m^{-2} s^{-1} at 14:30. The flux in the afternoon period fluctuated around -0.3 μmol m^{-2} s^{-1}. The fitted sinusoidal curve reached its minimum at about 16:00, 4 h after solar radiation peaked. From November to January, the flux ranged from -0.032 μmol m^{-2} s^{-1} (21:00) to 0.356 μmol m^{-2} s^{-1} (09:00).

https://doi.org/10.5194/egusphere-2026-6709
Preprint. Discussion started: 16 November 2026
© Author(s) 2026. CC BY 4.0 License.

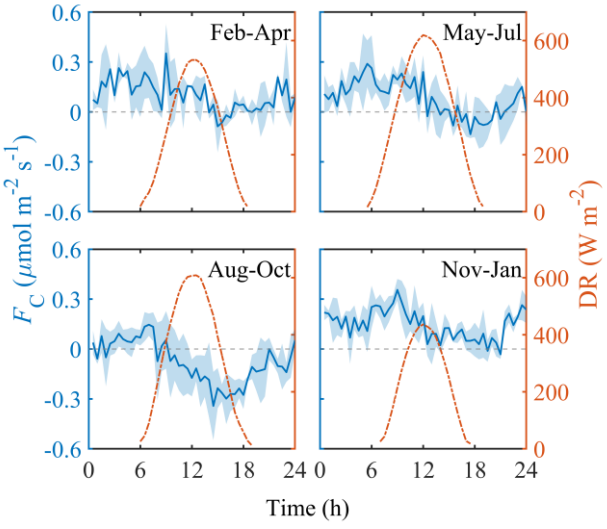


Figure 7. Composite diurnal patterns of CO_2 flux (F_C) and downward solar radiation (DR) in the four seasonal phases. Shaded areas are ±1 standard deviation of CO_2 flux across years.

At the monthly scale, the SAV zone acted as a net CO_2 source during the winter and the spring and a sink in the late summer to the early autumn (Fig. 8a). The most positive monthly flux (0.230 μmol m^{-2} s^{-1}) was recorded in December 2023 and the most negative flux (-0.189 μmol m^{-2} s^{-1}) in August 2023. The monthly CO_2 flux showed interannual differences in the length of uptake period, in the timing of the transition from net emission to net uptake, and in the magnitude of CO_2 uptake. In 2020, the net CO_2 uptake was observed only in October. In 2022 and 2023, the uptake period persisted for three months from August to October. The sign transition occurred in July in 2023 and between July and August in 2022. The peak uptake flux varied from -0.079 μmol m^{-2} s^{-1} in 2021 (September) to -0.189 μmol m^{-2} s^{-1} in 2023 (August).

The cumulative CO_2 flux is shown in Fig. 8b for 2022 and 2023, the years with the most complete data coverage. In both years, the annual flux was positive, at 45 and 89 g CO_2 m^{-2}, respectively, indicating that this SAV habitat acted overall as a net source of atmospheric CO_2. The cumulative uptake in August to October was 33 g CO_2 m^{-2} in 2022 and 60 g CO_2 m^{-2} in 2023, but this amount was not enough to offset the cumulative emission in the other months.

https://doi.org/10.5194/egusphere-2026-6709
Preprint. Discussion started: 16 November 2026
© Author(s) 2026. CC BY 4.0 License.

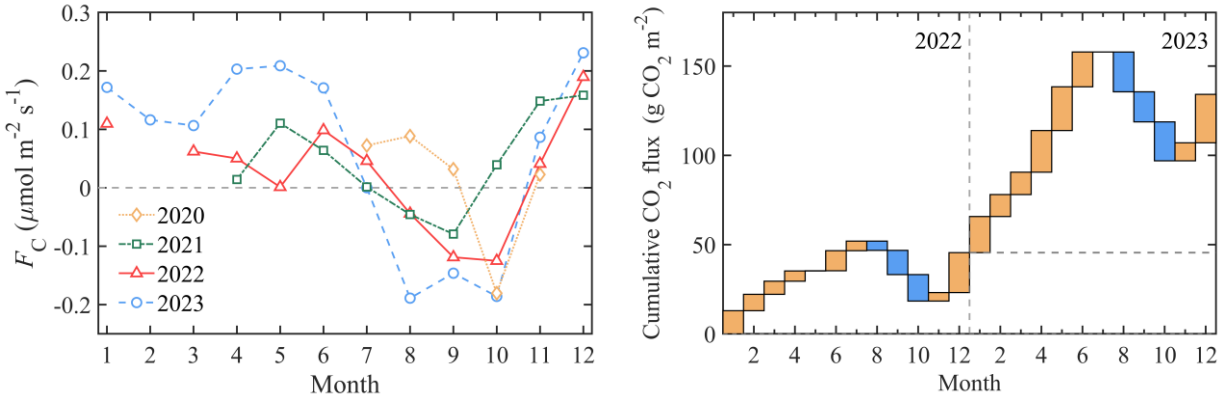


Figure 8. Seasonal variations in the monthly mean CO_2 flux (a) and the cumulative flux (b). In panel b, orange and blue colors indicate positive and negative monthly mean flux, respectively.

3.3 Relationships with environmental conditions

Water temperature (Tw) and solar radiation (DR) are two biological relevant variables. They displayed large diurnal and seasonal variations (Fig. S4). At the half-hourly time scale, the CO_2 flux showed no dependence on these two variables (Fig. S5). At the daily scale, individual observations were highly scattered. After bin averaging, the daily mean CO_2 flux decreased with increasing Tw in both vegetation-index groups (Fig. 9a). The fitted relationships were $y = -0.0031x + 0.1397$ ($R^2 = 0.33$) for months with $\Delta NDVI < 0.2$ and $y = -0.0057x + 0.0841$ ($R^2 = 0.15$) for months with $\Delta NDVI > 0.2$. The relationship between bin-averaged daytime CO_2 flux and solar radiation differed between the two groups (Fig. 9b). For months with $\Delta NDVI < 0.2$, the relationship was weakly negative ($y = -0.0001x + 0.0968$, $R^2 = 0.19$), whereas for months with $\Delta NDVI > 0.2$, it was positive ($y = 0.0002x - 0.2239$, $R^2 = 0.36$). Despite this positive slope, bin-averaged daytime flux remained negative across the observed radiation range in the higher-$\Delta NDVI$ group, indicating net daytime CO_2 uptake. No clear relationship was observed between the daily CO_2 flux and water depth (Fig. S6). However, the daily CO_2 flux tended to approach zero as water depth increased, whereas larger fluctuations occurred under shallower water conditions.

https://doi.org/10.5194/egusphere-2026-6709
Preprint. Discussion started: 16 November 2026
© Author(s) 2026. CC BY 4.0 License.

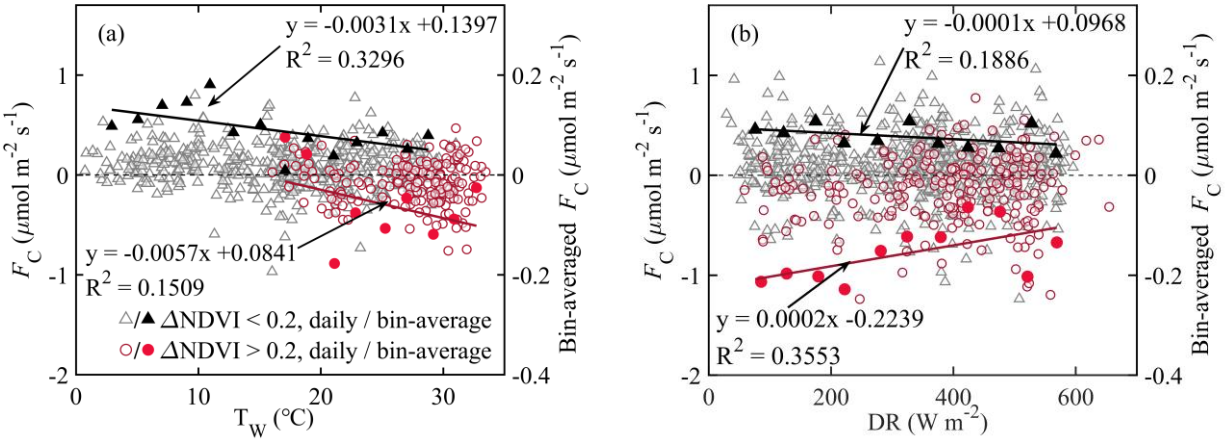


Figure 9. Relationships of CO_2 flux with environmental variables. (a) Daily mean flux with 20-cm water temperature. (b) Daytime mean flux with solar radiation. Open triangles and open circles represent data with monthly **Δ**NDVI < 0.2 and **Δ**NDVI > 0.2, respectively. Filled triangles and filled circles denote bin-averaged values with monthly **Δ**NDVI < 0.2 and **Δ**NDVI > 0.2, respectively. Lines are linear regression with regression statistics noted.

At the monthly scale, the flux became more negative with increasing water temperature and ΔNDVI (Fig. 10). The relationships with water depth and solar radiation were also negative, but the correlations were not statistically significant. The linear relationship with ΔNDVI was strongest; this variable explained 45 % of the variability in the observed monthly flux. A stepwise multiple regression analysis identified that among the four environmental variables shown in Fig. 10, ΔNDVI was the only significant predictor of F_C ($p < 0.001$). The final regression model yielded the following equation: $F_C = 0.108 - 0.563 \times \Delta NDVI$.

https://doi.org/10.5194/egusphere-2026-6709
Preprint. Discussion started: 16 November 2026
© Author(s) 2026. CC BY 4.0 License.

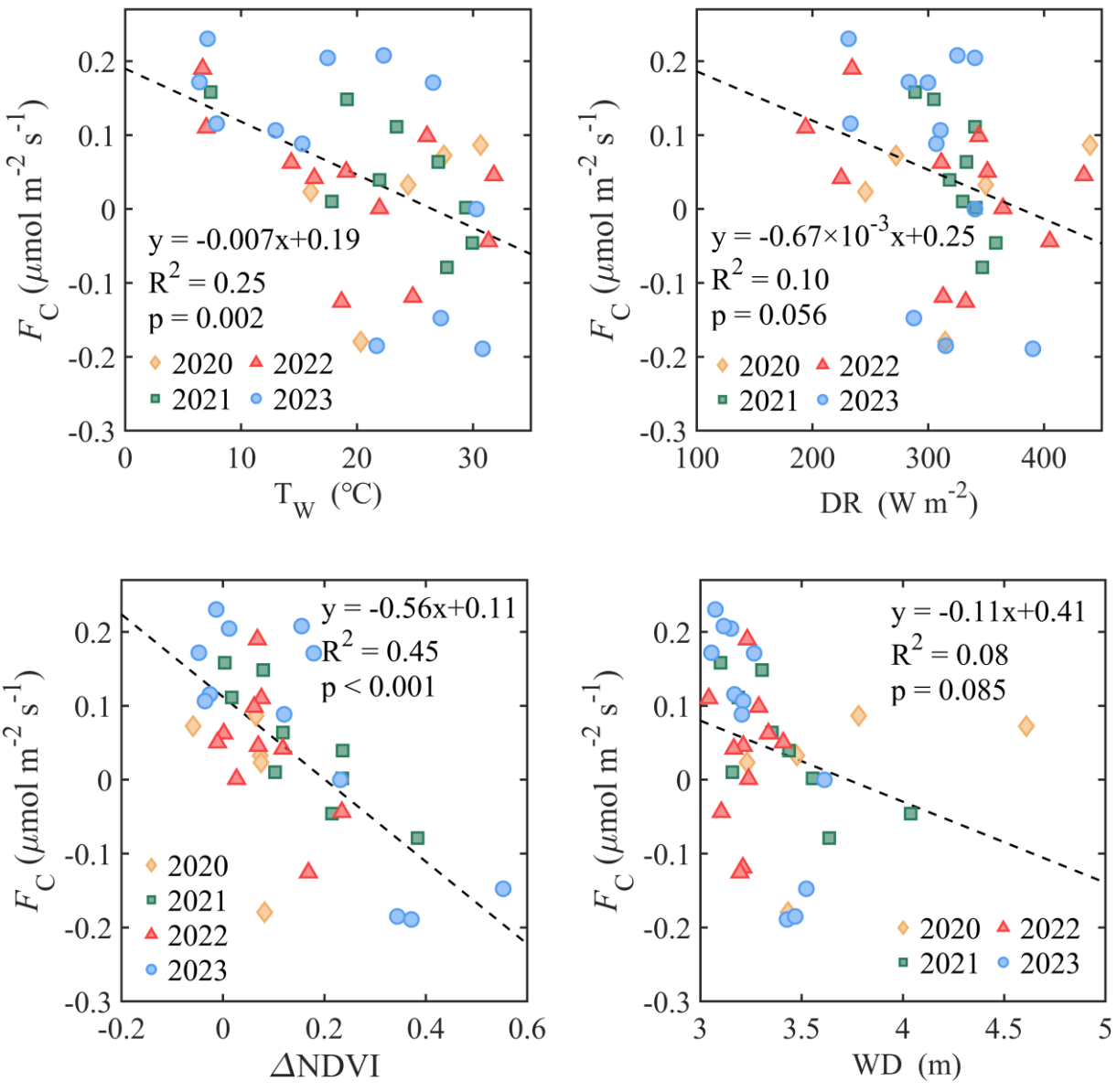


Figure 10. Relationship of monthly flux with 20-cm water temperature (T_W), solar radiation (DR), baseline-corrected NDVI, and water depth (WD). Lines are linear regression with regression statistics noted.

https://doi.org/10.5194/egusphere-2026-6709
Preprint. Discussion started: 16 November 2026
© Author(s) 2026. CC BY 4.0 License.

3.4 Dissolved CO_2 concentration and net ecosystem exchange

Fig. 11 shows the dissolved CO_2 concentration observed in 2020. The concentration ranged from 7.06 to 47.54 μmol L^{-1}. The interquartile range was 14.18 to 20.90 μmol L^{-1}, with a median of 16.76 μmol L^{-1}. Its probability density was positively skewed, with a peak at 14.96 μmol L^{-1} (Fig. 11a). The concentration was higher in the winter than in the summer (Fig. 11b). Panels c-e in Fig. 11 show the time series over three 10-day periods. During DOY 50–60 (February 19 to 29, 2020), the concentration generally increased throughout the night, reached a maximum at approximately 07:00, subsequently declined to a minimum at approximately 15:00, and then increased again after dusk (Fig. 11c). The mean diurnal amplitude was 10.39 μmol L^{-1}. During DOY 200–210 (July 18 to 28), the concentration exhibited only minor diurnal variability, with slightly elevated values at 06:00 and a minimum at 18:00 (Fig. 11d), with a mean diurnal amplitude of 1.75 μmol L^{-1}. The most pronounced diurnal variability occurred during DOY 270–280 (September 26 to October 6), with a minimum at 06:00, a maximum at 14:00 and a mean amplitude of 20.42 μmol L^{-1} (Fig. 11e).

https://doi.org/10.5194/egusphere-2026-6709
Preprint. Discussion started: 16 November 2026
© Author(s) 2026. CC BY 4.0 License.

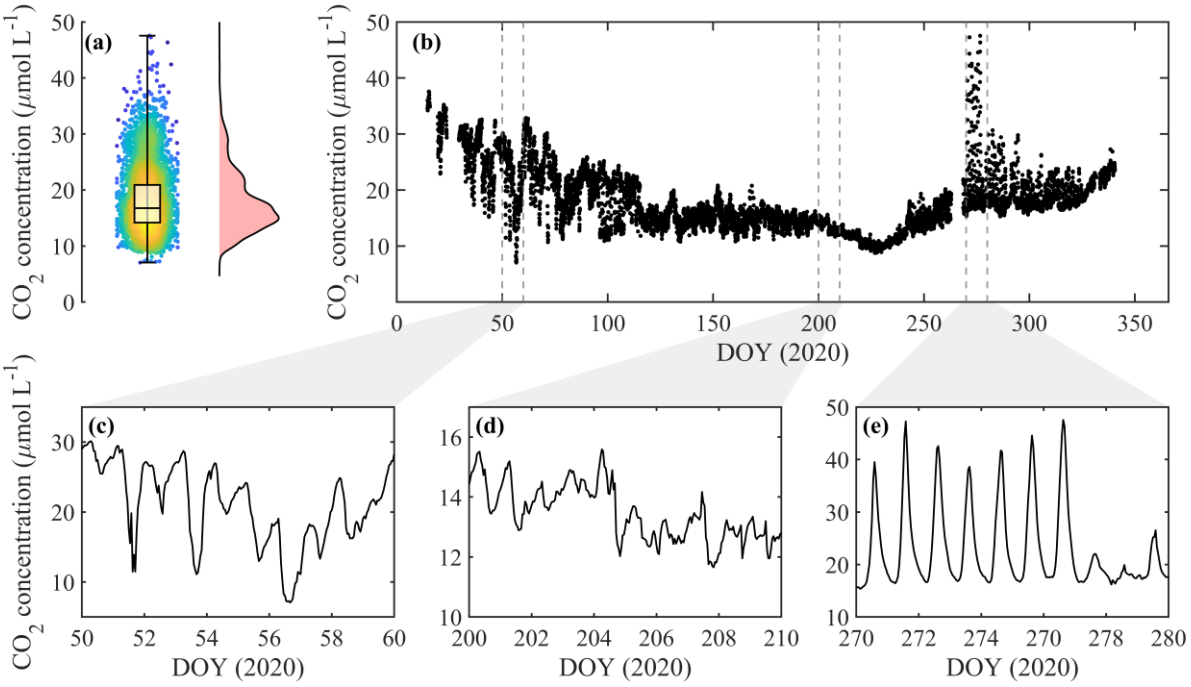


Figure 11. Statistical distribution and temporal dynamics of dissolved CO_2 concentration. (a) Distribution of the CO_2 concentration, with each data point representing an observation at hourly intervals, showing the probability density distribution (pink) and a box plot with the median (line), the 25th and 75th percentiles (box), and the lowest and highest observations within 1.5 × the interquartile range (IQR) of the box edges (whiskers). (b) Annual variation in the CO_2 concentration. (c–e) Detailed temporal variations in three 10-day periods.

Because of time variations in the dissolved CO_2 concentration, the CO_2 flux measured above the water surface was not the true net ecosystem exchange (NEE). In studies of land ecosystems, their relationship is given by

$$\mathrm{NEE} = F_C + F_{C,S} \quad (5)$$

where $F_{C,S}$ is the amount of change of CO_2 stored in the air column below the EC height over the observational period. The sign convention for the storage flux is that it is negative if the CO_2 concentration

https://doi.org/10.5194/egusphere-2026-6709
Preprint. Discussion started: 16 November 2026
© Author(s) 2026. CC BY 4.0 License.

is lower at the end than at the beginning of an observational period and is positive otherwise. The storage flux sums to zero over periods longer than a day but can be important at sub-day time scales.

We applied this framework here to estimate the influence of CO_2 storage in the water column. In this application, the concentration measured at the 20-cm depth was assumed to represent the mean of the full water column and the storage in the air column between the water surface and the EC height was ignored. The calculation was done for the period from August to October 2020, the growth period with peak SAV coverage. Figure 12 shows the diurnal composites of the three terms in Eq. (5). The diurnal variation in $F_{C,S}$ was greater than that in F_C. NEE exhibited a temporal pattern broadly consistent with that of $F_{C,S}$, reaching a daily maximum of 0.770 μmol m^{-2} s^{-1} at 11:00 and a daily minimum of -0.723 μmol m^{-2} s^{-1} at 17:00 which is about 5 h behind the solar radiation peak. The close correspondence between NEE and the storage flux is the main reason for why Fc was not responsive to changes in environmental conditions at hourly to sub-day time scales (Fig. S5).

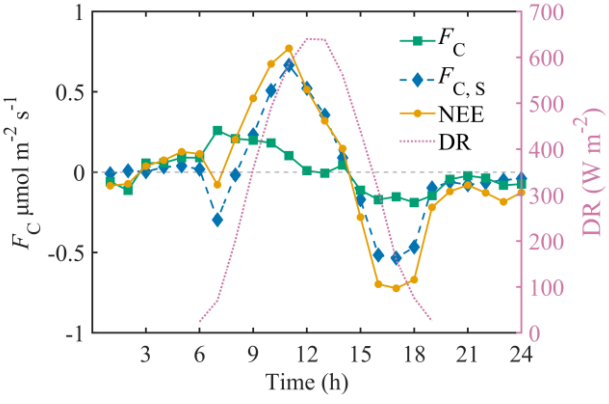


Figure 12. Mean diurnal variations of water–air CO_2 flux (F_C), CO_2 storage flux ($F_{C,S}$), net ecosystem CO_2 exchange (NEE) and downward solar radiation (DR) from August to October, 2020.

4 Discussion

4.1 Comparison with other observations in Lake Taihu

Several research groups have measured the CO_2 flux at Lake Taihu using flux chambers and the gas transfer coefficient method. Fig. 13 compare their results with our data for 2022 and 2023, the two years

https://doi.org/10.5194/egusphere-2026-6709
Preprint. Discussion started: 16 November 2026
© Author(s) 2026. CC BY 4.0 License.

with minimal data gaps (Fig. 8). The annual mean flux in this study was 0.033 μmol m^{-2} s^{-1} (2.851 mmol m^{-2} d^{-1}) in 2022 and 0.064 μmol m^{-2} s^{-1} (5.530 mmol m^{-2} d^{-1}) in 2023, indicating that the SAV ecosystem was a weak atmospheric CO_2 source when averaged over the full year. These flux values fall in between those observed with flux chambers and the transfer coefficient method. The chamber observation by Zhang et al. (2024) indicates net CO_2 uptake in various aquatic zones across the lake. Notably, their annual mean flux in a SAV zone near our site was negative, at -2.54 mmol m^{-2} d^{-1}. Part of this discrepancy may be explained by temporal representativeness. Although the chamber method was employed at multiple points, the sampling frequency was limited to a single daytime observation per month, potentially biasing the annual estimate towards periods of photosynthetic uptake and therefore more negative values.

In contrast, studies using the transfer coefficient approach generally show that Lake Taihu is a net source of atmospheric CO_2. These studies were conducted in a range of functional zones of the lake. Measurements by Xiao et al. (2020, 2021, 2022) in eutrophic pelagic areas, central open waters, and the eastern aquatic vegetation (AV) zone of Lake Taihu indicated net CO_2 emissions of 12.40–20.0 mmol m^{-2} d^{-1}, with a mean flux of 13.84 mmol m^{-2} d^{-1} in the SAV zone. Hong et al. (2025) reported comparable results, with an annual mean flux of 13.55 mmol m^{-2} d^{-1} in SAV areas. Fan et al. (2005) reported a near-zero and slightly negative annual mean CO_2 flux for a SAV zone, which was lower than the estimates for the other lake regions.

https://doi.org/10.5194/egusphere-2026-6709
Preprint. Discussion started: 16 November 2026
© Author(s) 2026. CC BY 4.0 License.

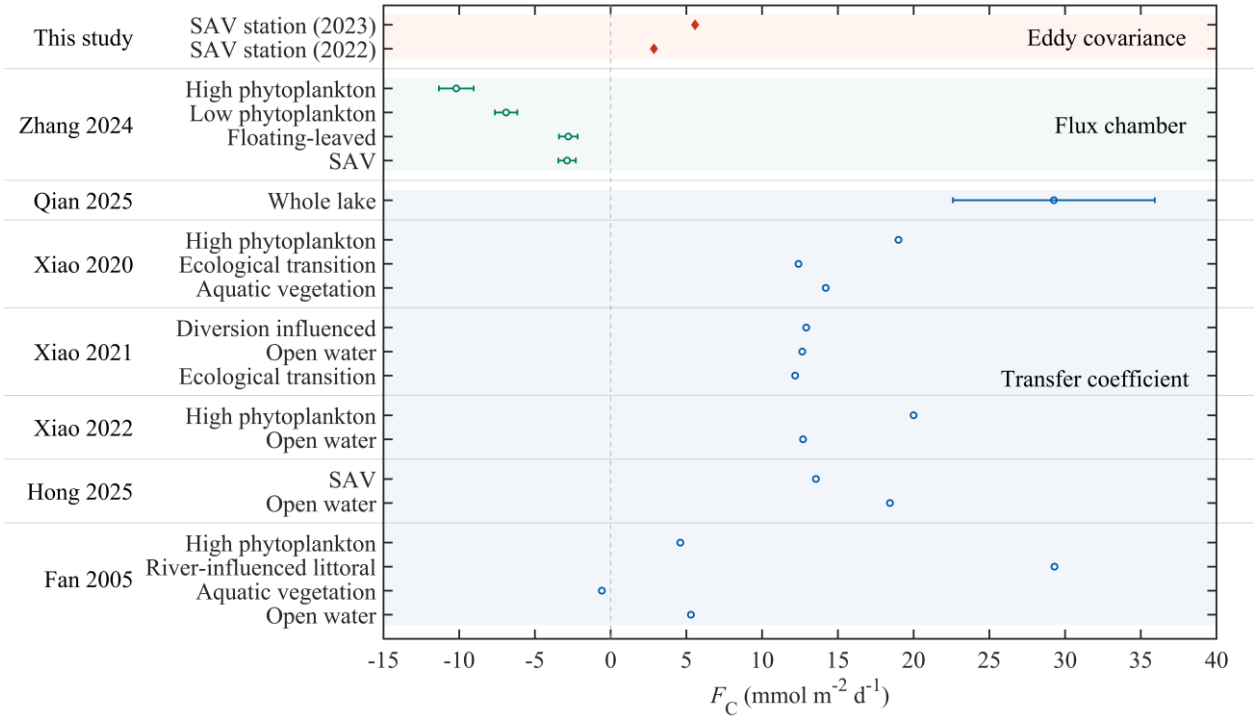


Figure 13. Comparison of air–water CO_2 flux measured in this study with those previously reported for Lake Taihu based on flux-chamber or transfer-coefficient methods. Only studies with observation periods covering at least one full year are included. Error bars indicate ±1 standard deviation of spatial replicates.

The seasonal pattern in this study was characterized by CO_2 emission during senescence (November to January) and moderate uptake during peak SAV coverage (August to October; Fig. 7). This seasonal progression is consistent with open-water and SAV studies showing greater CO_2 emissions during the cold season than during the summer (Qian et al., 2025; Hong et al., 2025). This pattern results from enhanced macrophyte and phytoplankton photosynthesis in the growing season. Additionally, the CO_2 flux in this study exhibited weak nighttime emission from August to October, transitioning to uptake after sunrise and reaching its maximum uptake in the afternoon, while in other months, diurnal variations were relatively weak (Fig. 6). Similar to this study, observations by Shen et al. (2024) at 3-hour intervals using the transfer coefficient method in a SAV zone in East Taihu Lake showed that the lake was a CO_2 sink

https://doi.org/10.5194/egusphere-2026-6709
Preprint. Discussion started: 16 November 2026
© Author(s) 2026. CC BY 4.0 License.

during the daytime and a CO_2 source at night in the summer, whereas it was a source during the day and at night in the autumn.

4.2 Comparison with other lake observations

The weak net annual CO_2 emission observed in this study was comparable in magnitude to those reported for SAV-covered areas of Lake Biandantang in Hubei Province, central China, and Lake Xuanwu in Nanjing, eastern China, where the annual mean CO_2 fluxes were 1.96 and 2.61 mmol m^{-2} d^{-1}, respectively (Xing et al., 2006; Diao et al., 2025). In the SAV-dominated area of Lake Ulansuhai in western Inner Mongolia, China, the annual mean CO_2 flux was 6.17 mmol m^{-2} d^{-1}, slightly higher than that observed in this study (Li et al., 2022). Substantially greater emission was observed for macrophyte-dominated Lake Schulzensee in northeastern Germany, with an annual mean CO_2 flux of 21.92 mmol m^{-2} d^{-1} (Brothers et al., 2013). Conversely, SAV-dominated shallow lakes on the Pampean Plain of central-eastern Argentina acted as net CO_2 sinks, with an annual mean CO_2 flux of −1.8 mmol m^{-2} d^{-1} (Baliña et al., 2023). These observations indicate that SAV-dominated lakes can function as either CO_2 sources or sinks. Differences in climatic conditions (Kosten et al., 2010) and in the supply and storage of inorganic carbon within the water column (Andersen et al., 2019; Martinsen et al., 2022) may contribute to this variability. Seasonal changes in SAV biomass, growth and decomposition may also affect the balance between CO_2 consumption and production and contribute to differences in annual CO_2 flux among lakes.

SAV-dominated lakes commonly exhibit a distinct seasonal pattern, with CO_2 uptake during periods of active plant growth and CO_2 emissions during periods of reduced growth or colder conditions (Jeppesen et al., 2016; Rõõm et al., 2014). However, CO_2 uptake by SAV during the growing season does not necessarily cause a net uptake at the annual scale. In Lake Lacanau in southwestern France, for example, summer CO_2 emissions were substantially lower than those in other seasons because of enhanced plant CO_2 consumption, and the annual mean CO_2 flux remained slightly positive (Ribaudo et al., 2018). Furthermore, the seasonal window of net CO_2 uptake varies among SAV-dominated lakes. In SAV areas of Lake Biandantang, the CO_2 uptake period extended from May to November (Xing et al., 2006), representing a longer seasonal window of net uptake than that observed in this study. Lakes La Segunda

https://doi.org/10.5194/egusphere-2026-6709
Preprint. Discussion started: 16 November 2026
© Author(s) 2026. CC BY 4.0 License.

and Kakel Huincul on the Pampean Plain exhibited net CO_2 uptake during spring and summer (Baliña et al., 2023) indicating an earlier seasonal uptake pattern than in this study.

In this study, during August–October, when SAV coverage was relatively high, CO_2 uptake was strongest in the afternoon. This photosynthesis-driven daytime CO_2 consumption appears to be a common diurnal feature of SAV-dominated lakes (Andersen et al., 2019; Guo et al., 2026). A difference among these lakes is the direction of nighttime CO_2 exchange. In this study, the mean diurnal pattern from August to October showed weak nighttime CO_2 emissions overall, although nighttime uptake was also observed during some periods. In Lake Nymølle in eastern Denmark, diurnal changes in dissolved CO_2 concentration during summer likewise indicated a transition from daytime CO_2 uptake to nighttime emission (Martinsen et al., 2022). By contrast, the SAV-covered area of Lake Ulansuhai continued to exhibit CO_2 uptake at night, with nighttime uptake accounting for 25–45% of total daily CO_2 uptake (Zhang et al., 2022). These contrasting nighttime patterns highlight the importance of observation over the full diurnal cycle when assessing daily and longer-term CO_2 budgets.

4.3 The role of CO_2 storage and diffusion limitation

During the peak SAV period, the CO_2 uptake from the atmosphere was strongest 4 h after solar radiation had reached its maximum (Fig. 7). The diurnal amplitude of the aquatic CO_2 storage flux was greater than that of the air–water interface flux, and the temporal pattern of NEE was more closely aligned with the storage flux (Fig. 12). These observations suggest that photosynthetic carbon demand was primarily accommodated by the dissolved CO_2 pool in the water column and was supplemented by CO_2 diffused from the atmosphere. The water column acted as a carbon reservoir, attenuating and delaying the expression of underwater biological activity in the above-water CO_2 flux over the diurnal cycle. This buffering explains why the flux was poorly correlated with solar radiation and water temperature at half-hourly to sub-day time scales (Fig. S5).

The large role of the storage term in NEE in this aquatic ecosystem contrasts sharply with that in land ecosystems. In land ecosystems, the storage term is consequential only during sunrise and sunset

https://doi.org/10.5194/egusphere-2026-6709
Preprint. Discussion started: 16 November 2026
© Author(s) 2026. CC BY 4.0 License.

transitions, and its magnitude is typically much smaller than the eddy flux itself. For example, the storage flux is −2.5 μmol m^{-2} s^{-1} at sunrise, +1.5 μmol m^{-2} s^{-1} at sunset, and negligible at other times of the day, during the growing season of a maize crop (Raza et al., 2026). Even during the transitional times of the day, the storage flux is one order of magnitude smaller than the typical midday CO_2 flux of maize crops (Suyker et al., 2004).

It is thought that reduction in water depth should bring SAV canopy closer to the water surface, allowing atmospheric CO_2 to be more readily available for photosynthesis (Watanabe and Kuwae, 2015; Maberly and Madsen, 2002). Although no direct relationship was detected between the daily mean flux and water depth (Fig. S6), the largest uptake in months of the highest NDVI (Fig. 10) could be partially attributed to the fact that at these times, the canopy was present near the water surface (Fig. 1 and Fig. S1) and therefore had easier access to atmospheric CO_2. It is worth noting that the largest uptake over the diurnal cycle in the peak SAV season occurred in later afternoon when the surface water was stably stratified (Fig. 4), which should have severely limited turbulent diffusion. Having the canopy close to the surface would overcome this diffusion barrier. It seems that the growth of SAV is self-perpetuating: a larger SAV canopy allows more foliage area for carbon capture and at the same time overcomes the diffusion limitation by being closer to the surface.

4.4 Evidence for CAM

The flux observed during peak SAV coverage (August to October) provided some evidence for CAM. In this growth stage, the lake exhibited only weak nighttime CO_2 emission (flux being positive) and, in some cases, net CO_2 uptake (flux being negative; Fig. 6). The mean nighttime flux was negative in about 50% of the days in this period. In 2023, the monthly mean nighttime CO_2 flux was −0.079, −0.008, and −0.111 μmol m^{-2} s^{-1}, in August, September and October, respectively. Outside this period, the fraction of negative nighttime flux was lower, at about 30%, and the monthly mean nighttime flux ranged from 0.102 to 0.301 μmol m^{-2} s^{-1}. As mentioned earlier, at times of peak growth, the SAV extended its foliage close to the water surface. During this time, the growth appeared to be partially supported by the nighttime acquisition of atmospheric CO_2.

https://doi.org/10.5194/egusphere-2026-6709
Preprint. Discussion started: 16 November 2026
© Author(s) 2026. CC BY 4.0 License.

The species composition of the SAV community in Lake Taihu provides some ecological basis for this interpretation. *Potamogeton malaianus*, a dominant species in the submerged macrophyte zone of Lake Taihu, exhibits diurnal variations in titratable acidity, which is indicative of a CAM-like pattern (Yin et al., 2017). *Vallisneria natans* and *Myriophyllum spicatum L.* have been recorded in Xukou Bay, where the BFG site is located (Dong et al., 2017; Zhao, 2017). CAM activity has also been reported in *V. natans* under low-CO_2 conditions (Liao et al., 2026) and in *M. spicatum* at Tibetan Plateau sampling sites (J. Jia et al., 2024).

An alternative interpretation for the negative nighttime flux is passive CO_2 diffusion. It is possible that the daytime underwater photosynthesis caused the partial pressure of CO_2 in the water to be lower than in the atmosphere at sunset. This pressure gradient would cause CO_2 to diffuse downward from the atmosphere to the water column. However, the changes in dissolved CO_2 concentration at night supports the CAM interpretation. During the peak SAV coverage in 2020, the dissolved CO_2 concentration declined continuously between 20:00 and 24:00 resulting in a negative storage flux, and subsequently began to increase resulting in a positive storage flux (Fig. 12). The NEE was negative between 20:00 and 02:00 (mean value -0.114 μmol m^{-2} s^{-1}) and positive between 3:00 and 4:00 (mean value + 0.056 μmol m^{-2} s^{-1}). This pattern indicated dark-period CO_2 fixation during the first half of the night. As malic acid storage capacity, phosphoenolpyruvate substrate availability, or external CO_2 availability declined, CAM fixation may have weakened during the second half of the night, allowing ecosystem respiration to become dominant (Keeley and Bowes, 1982; Klavsen and Maberly, 2010).

5 Conclusions

In this study, we used eddy covariance observation from July 2020 to December 2023 to investigate the CO_2 exchange between a SAV habitat of Lake Taihu and the atmosphere. The habitat acted as a weak atmospheric CO_2 source on the annual time scale, with a net emission of 45 and 89 g CO_2 m^{-2} yr^{-1} in 2022 and 2023, respectively. A distinct seasonal transition was observed from net CO_2 emission during the winter and the spring to net uptake in the late summer and the early autumn.

https://doi.org/10.5194/egusphere-2026-6709
Preprint. Discussion started: 16 November 2026
© Author(s) 2026. CC BY 4.0 License.

The relationship between CO_2 flux and environmental conditions depended on the choice of time scale. At the monthly scale, the baseline-corrected NDVI explained 45% of the observed flux variability and was the only significant predictor retained by stepwise multiple linear regression among vegetation index, water temperature, solar radiation, and water depth. At the half-hourly scale, the flux showed no clear dependence on solar radiation or water temperature. No clear direct relationship was found between the daily mean flux and water depth.

During peak SAV coverage, the strongest atmospheric CO_2 uptake occurred approximately 4 h after the solar radiation maximum. The water-column CO_2 storage flux had a greater diurnal amplitude than the air–water interface (eddy) flux. These observations suggest that the dissolved CO_2 pool buffered carbon exchange and delayed the expression of underwater biological activity in the above-water flux.

Nighttime atmospheric CO_2 uptake was observed during some periods of peak SAV coverage. From August to October 2020, the decline in dissolved CO_2 during the first half of the night and the negative net ecosystem exchange provided some evidence for CAM activity. Our results indicate that water-column CO_2 storage needs to be considered when interpreting above-water flux measurements in terms of SAV carbon uptake.

Code and data availability

Codes for processing the data figures are available from the authors upon request. Observational data is available at Figshare (https://figshare.com/s/de9090b2e2d7dd6dee09).

Author contributions

LJ conducted the investigation, performed the formal analysis, and wrote the original manuscript draft. MZ and WX supervised the research, administered the project, and secured funding. YP and ZZ contributed to establishing the observation site and installing the monitoring instruments. PG, FY, HB,

https://doi.org/10.5194/egusphere-2026-6709
Preprint. Discussion started: 16 November 2026
© Author(s) 2026. CC BY 4.0 License.

and YH curated the data. XL conceptualized the study, developed the methodology, and reviewed and edited the manuscript.

Competing interests

The authors declare no conflict of interest.

Disclaimer

Copernicus Publications remains neutral with regard to jurisdictional claims made in the text, published maps, institutional affiliations, or any other geographical representation in this paper. While Copernicus Publications makes every effort to include appropriate place names, the final responsibility lies with the authors. Views expressed in the text are those of the authors and do not necessarily reflect the views of the publisher.

Acknowledgements

We acknowledge the faculty members and students who contributed to the long-term operation and maintenance of the Lake Taihu Eddy Flux Mesonet. We thank Yanlei Li and Shanggang Li, engineers at Campbell Scientific, for their technical support with the installation, troubleshooting, and maintenance of the eddy covariance system. We also thank Qitao Xiao for providing additional details and numerical data from his published work, which supported the comparative analysis presented in this study.

Financial support

This research has been supported by the National Natural Science Foundation of China (42021004 & 41575147), the R&D Foundation of Jiangsu Province, China (BK20220020), the National Key R&D Program of China (2020YFA0607501), the Natural Science Foundation of Jiangsu Province for

https://doi.org/10.5194/egusphere-2026-6709
Preprint. Discussion started: 16 November 2026
© Author(s) 2026. CC BY 4.0 License.

Distinguished Young Scholars (BK20220055), the Foundation of Jiangsu Key Laboratory of Severe Storm Disaster Risk (QDL2026Q04).

References

Adamec, L.: Ecophysiological characteristics of turions of aquatic plants: A review, Aquat. Bot., 148, 64–77, https://doi.org/10.1016/j.aquabot.2018.04.011, 2018.

Aho, K. S., Hosen, J. D., Logozzo, L. A., McGillis, W. R., and Raymond, P. A.: Highest rates of gross primary productivity maintained despite CO_2 depletion in a temperate river network, Limnol. Oceanogr. Lett., 6, 200–206, https://doi.org/10.1002/lol2.10195, 2021.

Andersen, M. R., Kragh, T., Martinsen, K. T., Kristensen, E., and Sand-Jensen, K.: The carbon pump supports high primary production in a shallow lake, Aquat. Sci., 81, 24, https://doi.org/10.1007/s00027-019-0622-7, 2019.

Baattrup-Pedersen, A., Madsen, T. V., Riis, T., and Cavalli, G.: Photosynthetic performance of submerged macrophytes from lowland stream and lake habitats with contrasting CO_2 availability, New Phytol., 198, 1135–1142, https://doi.org/10.1111/nph.12203, 2013.

Bakker, E. S., Wood, K. A., Pagès, J. F., Veen, G. F., Christianen, M. J. A., Santamaría, L., Nolet, B. A., and Hilt, S.: Herbivory on freshwater and marine macrophytes: a review and perspective, Aquat. Bot., 135, 18–36, https://doi.org/10.1016/j.aquabot.2016.04.008, 2016.

Baliña, S., Sánchez, M. L., Izaguirre, I., and del Giorgio, P. A.: Shallow lakes under alternative states differ in the dominant greenhouse gas emission pathways, Limnol. Oceanogr., 68, 1–13, https://doi.org/10.1002/lno.12243, 2023.

Brothers, S. M., Hilt, S., Attermeyer, K., Grossart, H. P., Kosten, S., Lischke, B., Mehner, T., Meyer, N., Scharnweber, K., and Köhler, J.: A regime shift from macrophyte to phytoplankton dominance enhances carbon burial in a shallow, eutrophic lake, Ecosphere, 4, 1–17, https://doi.org/10.1890/es13-00247.1, 2013.

Carpenter, S. R.: Submersed vegetation: an internal factor in lake ecosystem succession, Am. Nat., 118, 372–383, https://doi.org/10.1086/283829, 1981.

https://doi.org/10.5194/egusphere-2026-6709
Preprint. Discussion started: 16 November 2026
© Author(s) 2026. CC BY 4.0 License.

Diao, F., Qiu, W., Zhang, D., Wu, Z., Guan, B., Xing, P., Feng, M., Zhang, Y., Su, Y., and Li, K.: Contrasting greenhouse gas flux responses to ecological restoration: comparative insights from two shallow lakes, J. Environ. Manage., 396, 128124, https://doi.org/10.1016/j.jenvman.2025.128124, 2025.

Dong, B., Qin, B., Li, W., and Gao, G.: Growth and community composition of submerged macrophytes in Lake Taihu (China): Assessment of changes in response to sediment characteristics, Wetlands, 37, 233–243, https://doi.org/10.1007/s13157-016-0861-5, 2017.

Ersoy, Z., Scharfenberger, U., Baho, D. L., Bucak, T., Feldmann, T., Hejzlar, J., Levi, E. E., Mahdy, A., Nõges, T., Papastergiadou, E., Stefanidis, K., Šorf, M., Søndergaard, M., Trigal, C., Jeppesen, E., and Beklioğlu, M.: Impact of nutrients and water level changes on submerged macrophytes along a temperature gradient: A pan-European mesocosm experiment, Glob. Change Biol., 26, 6831–6851, https://doi.org/10.1111/gcb.15338, 2020.

Fan, C., Hu, W., Ford, P. W., Chen, Y., Qu, W., and Zhang, L.: Carbon dioxide partial pressure and carbon fluxes of air-water interface in Taihu Lake, China, Chin. J. Oceanol. Limnol., 23, 29–38, https://doi.org/10.1007/bf02845140, 2005.

Foken, T., Leuning, R., Oncley, S. R., Mauder, M., and Aubinet, M.: Corrections and data quality control, in: Eddy Covariance: A Practical Guide to Measurement and Data Analysis, edited by: Aubinet, M., Vesala, T., and Papale, D., Springer, Dordrecht, 85–131, https://doi.org/10.1007/978-94-007-2351-1_4, 2012.

G.-Tóth, L., Parpala, L., Balogh, C., Tátrai, I., and Baranyai, E.: Zooplankton community response to enhanced turbulence generated by water-level decrease in Lake Balaton, the largest shallow lake in Central Europe, Limnol. Oceanogr., 56, 2211–2222, https://doi.org/10.4319/lo.2011.56.6.2211, 2011.

Golub, M., Koupaei-Abyazani, N., Vesala, T., Mammarella, I., Ojala, A., Bohrer, G., Weyhenmeyer, G. A., Blanken, P. D., Eugster, W., Koebsch, F., Chen, J., Czajkowski, K., Deshmukh, C., Guérin, F., Heiskanen, J., Humphreys, E., Jonsson, A., Karlsson, J., Kling, G., Lee, X., Liu, H., Lohila, A., Lundin, E., Morin, T., Podgrajsek, E., Provenzale, M., Rutgersson, A., Sachs, T., Sahlée, E., Serça, D., Shao, C., Spence, C., Strachan, I. B., Xiao, W., and Desai, A. R.: Diel, seasonal, and inter-annual variation in carbon dioxide effluxes from lakes and reservoirs, Environ. Res. Lett., 18, 034046, https://doi.org/10.1088/1748-9326/acb834, 2023.

https://doi.org/10.5194/egusphere-2026-6709
Preprint. Discussion started: 16 November 2026
© Author(s) 2026. CC BY 4.0 License.

Guo, R., Guo, C., Ke, J., Xiang, Y., Guo, K., Deng, C., Shi, X., Zhang, T., Liu, J., and Li, W.: Diurnal variation in water-air greenhouse gas fluxes across different aquatic vegetation habitats in a shallow subtropical lake, Water, 18, 557, https://doi.org/10.3390/w18050557, 2026.

Hilt, S., Gross, E. M., Hupfer, M., Morscheid, H., Mählmann, J., Melzer, A., Poltz, J., Sandrock, S., Scharf, E.-M., Schneider, S., and van de Weyer, K.: Restoration of submerged vegetation in shallow eutrophic lakes – A guideline and state of the art in Germany, Limnologica, 36, 155–171, https://doi.org/10.1016/j.limno.2006.06.001, 2006.

Hong, L., Hu, C., Jiang, M., Shi, X., Luo, J., and Xiao, Q.: Long-term carbon dioxide dynamics variability at submerged macrophyte habitat of a subtropical shallow lake, J. Hydrol., 662, 133950, https://doi.org/10.1016/j.jhydrol.2025.133950, 2025.

Horst, T. W. and Lenschow, D. H.: Attenuation of scalar fluxes measured with spatially-displaced sensors, Bound.-Lay. Meteorol., 130, 275–300, https://doi.org/10.1007/s10546-008-9348-0, 2009.

Jeppesen, E., Trolle, D., Davidson, T. A., Bjerring, R., Søndergaard, M., Johansson, L. S., Lauridsen, T. L., Nielsen, A., Larsen, S. E., and Meerhoff, M.: Major changes in CO_2 efflux when shallow lakes shift from a turbid to a clear water state, Hydrobiologia, 778, 33–44, https://doi.org/10.1007/s10750-015-2469-9, 2016.

Jia, J., Jiang, H., Zhu, X., Wang, S., Wang, L., Liu, C., Li, W., and Huang, W.: Inorganic carbon utilization strategies of plateau aquatic plants in response to native habitats, Photosynth. Res., 162, 47–62, https://doi.org/10.1007/s11120-024-01115-4, 2024.

Jia, L., Zhang, M., Xiao, W., Pu, Y., Zhang, Z., Bao, H., Ge, P., Shi, J., He, Y., Yang, F., Aho, K., Raymond, P., and Lee, X.: Aerosol interference with open-path eddy covariance measurement in a lake environment, Agric. For. Meteorol., 355, 110104, https://doi.org/10.1016/j.agrformet.2024.110104, 2024.

Keeley, J. E.: CAM photosynthesis in submerged aquatic plants, Bot. Rev., 64, 121–175, https://doi.org/10.1007/bf02856581, 1998.

Keeley, J. E. and Bowes, G.: Gas exchange characteristics of the submerged aquatic crassulacean acid metabolism plant, *Isoetes howellii*, Plant Physiol., 70, 1455–1458, https://doi.org/10.1104/pp.70.5.1455, 1982.

https://doi.org/10.5194/egusphere-2026-6709
Preprint. Discussion started: 16 November 2026
© Author(s) 2026. CC BY 4.0 License.



Kelly, M. G., Thyssen, N., and Moeslund, B.: Light and the annual variation of oxygen- and carbon-based measurements of productivity in a macrophyte-dominated river, Limnol. Oceanogr., 28, 503–515, https://doi.org/10.4319/lo.1983.28.3.0503, 1983.

Klavsen, S. K. and Maberly, S. C.: Effect of light and CO_2 on inorganic carbon uptake in the invasive aquatic CAM-plant *Crassula helmsii*, Funct. Plant Biol., 37, 737–747, https://doi.org/10.1071/fp09281, 2010.

Klavsen, S. K., Madsen, T. V., and Maberly, S. C.: Crassulacean acid metabolism in the context of other carbon-concentrating mechanisms in freshwater plants: a review, Photosynth. Res., 109, 269–279, https://doi.org/10.1007/s11120-011-9630-8, 2011.

Kljun, N., Calanca, P., Rotach, M. W., and Schmid, H. P.: A simple two-dimensional parameterisation for Flux Footprint Prediction (FFP), Geosci. Model Dev., 8, 3695–3713, https://doi.org/10.5194/gmd-8-3695-2015, 2015.

Kosten, S., Roland, F., Da Motta Marques, D. M. L., Van Nes, E. H., Mazzeo, N., Sternberg, L. D. S. L., Scheffer, M., and Cole, J. J.: Climate-dependent CO_2 emissions from lakes, Global Biogeochem. Cy., 24, GB2007, https://doi.org/10.1029/2009gb003618, 2010.

Lee, X., Liu, S., Xiao, W., Wang, W., Gao, Z., Cao, C., Hu, C., Hu, Z., Shen, S., Wang, Y., Wen, X., Xiao, Q., Xu, J., Yang, J., and Zhang, M.: The Taihu eddy flux network: An observational program on energy, water, and greenhouse gas fluxes of a large freshwater lake, B. Am. Meteorol. Soc., 95, 1583–1594, https://doi.org/10.1175/bams-d-13-00136.1, 2014.

Li, G., Zhang, S., Shi, X., Zhan, L., Zhao, S., Sun, B., Liu, Y., Tian, Z., Li, Z., Arvola, L., Uusheimo, S., Tulonen, T., and Huotari, J.: Spatiotemporal variability and diffusive emissions of greenhouse gas in a shallow eutrophic lake in Inner Mongolia, China, Ecol. Indic., 145, 109578, https://doi.org/10.1016/j.ecolind.2022.109578, 2022.

Liao, Z., Bu, X., Li, W., Zhou, J., and Li, P.: Responses of CO_2 concentrating mechanisms to variable CO_2 in different leaf regions of *Vallisneria natans* and *V. spinulosa*, Sci. Rep., in press, https://doi.org/10.1038/s41598-026-64567-9, 2026.

https://doi.org/10.5194/egusphere-2026-6709
Preprint. Discussion started: 16 November 2026
© Author(s) 2026. CC BY 4.0 License.

Luo, J., Li, X., Ma, R., Li, F., Duan, H., Hu, W., Qin, B., and Huang, W.: Applying remote sensing techniques to monitoring seasonal and interannual changes of aquatic vegetation in Taihu Lake, China, Ecol. Indic., 60, 503–513, https://doi.org/10.1016/j.ecolind.2015.07.029, 2016.

Maberly, S. C. and Madsen, T. V.: Freshwater angiosperm carbon concentrating mechanisms: processes and patterns, Funct. Plant Biol., 29, 393–405, https://doi.org/10.1071/pp01187, 2002.

Martinsen, K. T., Zak, N. B., Baastrup-Spohr, L., Kragh, T., and Sand-Jensen, K.: Ecosystem metabolism and gradients of temperature, oxygen and dissolved inorganic carbon in the littoral zone of a macrophyte-dominated lake, J. Geophys. Res.-Biogeo., 127, e2022JG007193, https://doi.org/10.1029/2022jg007193, 2022.

McGillis, W. R., Edson, J. B., Hare, J. E., and Fairall, C. W.: Direct covariance air-sea CO_2 fluxes, J. Geophys. Res.-Oceans, 106, 16729–16745, https://doi.org/10.1029/2000jc000506, 2001.

Mo, K., Wang, C., Jin, Y., Shi, Z., Tian, Y., Jin, L., and Liu, C.: Seed bank contributions and environmental filtering shape seasonal dynamics and restoration potential of submerged macrophytes in Baiyangdian Lake, Front. Plant Sci., 17, 1830771, https://doi.org/10.3389/fpls.2026.1830771, 2026.

Moncrieff, J. B., Massheder, J. M., de Bruin, H., Elbers, J., Friborg, T., Heusinkveld, B., Kabat, P., Scott, S., Soegaard, H., and Verhoef, A.: A system to measure surface fluxes of momentum, sensible heat, water vapour and carbon dioxide, J. Hydrol., 188–189, 589–611, https://doi.org/10.1016/s0022-1694(96)03194-0, 1997.

Nobel, P. S. and Hartsock, T. L.: Relationships between photosynthetically active radiation, nocturnal acid accumulation, and CO_2 uptake for a Crassulacean acid metabolism plant, *Opuntia ficus-indica*, Plant Physiol., 71, 71–75, https://doi.org/10.1104/pp.71.1.71, 1983.

Owen, N. A., Ní Choncubhair, Ó., Males, J., del Real Laborde, J. I., Rubio-Cortés, R., Griffiths, H., and Lanigan, G.: Eddy covariance captures four-phase Crassulacean acid metabolism (CAM) gas exchange signature in *Agave*, Plant Cell Environ., 39, 295–309, https://doi.org/10.1111/pce.12610, 2016.

Pedersen, O., Colmer, T. D., and Sand-Jensen, K.: Underwater photosynthesis of submerged plants – recent advances and methods, Front. Plant Sci., 4, 140, https://doi.org/10.3389/fpls.2013.00140, 2013.

https://doi.org/10.5194/egusphere-2026-6709
Preprint. Discussion started: 16 November 2026
© Author(s) 2026. CC BY 4.0 License.

Podgrajsek, E., Sahlée, E., and Rutgersson, A.: Diel cycle of lake-air CO_2 flux from a shallow lake and the impact of waterside convection on the transfer velocity, J. Geophys. Res.-Biogeo., 120, 29–38, https://doi.org/10.1002/2014jg002781, 2015.

Pujol, D., Colomer, J., Serra, T., and Casamitjana, X.: Effect of submerged aquatic vegetation on turbulence induced by an oscillating grid, Cont. Shelf Res., 30, 1019–1029, https://doi.org/10.1016/j.csr.2010.02.014, 2010.

Qian, M., Zhou, Y., Zhou, L., Zhang, Y., Pu, Y., Drake, T. W., Davidson, T. A., Spencer, R. G. M., Brookes, J. D., and Jeppesen, E.: Inflow-modulated inputs of dissolved organic matter fuel carbon dioxide emissions from a large hyper-eutrophic lake, Water Res., 273, 123082, https://doi.org/10.1016/j.watres.2024.123082, 2025.

Raza, T., Hicks, B. B., Oetting, J. N., and Eash, N. S.: A simplified system to quantify storage of carbon dioxide, water vapor and heat within a maize canopy, Atmos. Meas. Tech., 19, 157–166, https://doi.org/10.5194/amt-19-157-2026, 2026.

Ribaudo, C., Tison-Rosebery, J., Buquet, D., Jan, G., Jamoneau, A., Abril, G., Anschutz, P., and Bertrin, V.: Invasive aquatic plants as ecosystem engineers in an oligo-mesotrophic shallow lake, Front. Plant Sci., 9, 1781, https://doi.org/10.3389/fpls.2018.01781, 2018.

Rõõm, E.-I., Nõges, P., Feldmann, T., Tuvikene, L., Kisand, A., Teearu, H., and Nõges, T.: Years are not brothers: Two-year comparison of greenhouse gas fluxes in large shallow Lake Võrtsjärv, Estonia, J. Hydrol., 519, 1594–1606, https://doi.org/10.1016/j.jhydrol.2014.09.011, 2014.

Sand-Jensen, K., Andersen, M. R., Martinsen, K. T., Borum, J., Kristensen, E., and Kragh, T.: Shallow plant-dominated lakes – extreme environmental variability, carbon cycling and ecological species challenges, Ann. Bot., 124, 355-366, https://doi.org/10.1093/aob/mcz084, 2019.

Scheffer, M.: Ecology of shallow lakes, Springer, Dordrecht, https://doi.org/10.1007/978-1-4020-3154-0, 2004.

Schloesser, D. W., Edsall, T. A., and Manny, B. A.: Growth of submersed macrophyte communities in the St. Clair-Detroit river system between Lake Huron and Lake Erie, Can. J. Bot., 63, 1061–1065, https://doi.org/10.1139/b85-145, 1985.

https://doi.org/10.5194/egusphere-2026-6709
Preprint. Discussion started: 16 November 2026
© Author(s) 2026. CC BY 4.0 License.

Shen, C., Qian, M., Song, Y., Chen, B., and Yang, J.: Surface pCO_2 and air-water CO_2 fluxes dominated by submerged aquatic vegetation: Implications for carbon flux in shallow lakes, J. Environ. Manage., 370, 122839, https://doi.org/10.1016/j.jenvman.2024.122839, 2024.

Shikhani, M., Reinschke, L., Aurich, P., Waldemer, C., Koschorreck, M., and Boehrer, B.: Composition of photosynthetic gas bubbles from submerged macrophytes, Water Resour. Res., 60, e2022WR034010, https://doi.org/10.1029/2022wr034010, 2024.

Suyker, A. E., Verma, S. B., Burba, G. G., Arkebauer, T. J., Walters, D. T., and Hubbard, K. G.: Growing season carbon dioxide exchange in irrigated and rainfed maize, Agric. For. Meteorol., 124, 1–13, https://doi.org/10.1016/j.agrformet.2004.01.011, 2004.

Tokoro, T., Hosokawa, S., Miyoshi, E., Tada, K., Watanabe, K., Montani, S., Kayanne, H., and Kuwae, T.: Net uptake of atmospheric CO_2 by coastal submerged aquatic vegetation, Glob. Change Biol., 20, 1873–1884, https://doi.org/10.1111/gcb.12543, 2014.

Verhofstad, M. J. J. M. and Bakker, E. S.: Classifying nuisance submerged vegetation depending on ecosystem services, Limnology, 20, 55–68, https://doi.org/10.1007/s10201-017-0525-z, 2019.

Ward, E. A., Aldis, C., Wade, T., Miliou, A., Tsimpidis, T., and Cameron, T. C.: Is all seagrass habitat equal? Seasonal, spatial, and interspecific variation in productivity dynamics within Mediterranean seagrass habitat, Front. Mar. Sci., 9, 891467, https://doi.org/10.3389/fmars.2022.891467, 2022.

Watanabe, K. and Kuwae, T.: Radiocarbon isotopic evidence for assimilation of atmospheric CO_2 by the seagrass Zostera marina, Biogeosciences, 12, 6251–6258, https://doi.org/10.5194/bg-12-6251-2015, 2015.

Webb, E. K., Pearman, G. I., and Leuning, R.: Correction of flux measurements for density effects due to heat and water vapour transfer, Q. J. Roy. Meteor. Soc., 106, 85–100, https://doi.org/10.1002/qj.49710644707, 1980.

Wetzel, R. G.: Limnology: Lake and River Ecosystems, 3rd ed., Academic Press, San Diego, ISBN 978-0-12-744760-5, https://doi.org/10.1016/C2009-0-02112-6, 2001.

Wilczak, J. M., Oncley, S. P., and Stage, S. A.: Sonic anemometer tilt correction algorithms, Bound.-Lay. Meteorol., 99, 127–150, https://doi.org/10.1023/a:1018966204465, 2001.

https://doi.org/10.5194/egusphere-2026-6709
Preprint. Discussion started: 16 November 2026
© Author(s) 2026. CC BY 4.0 License.

Winslow, L. A., Zwart, J. A., Batt, R. D., Dugan, H. A., Woolway, R. I., Corman, J. R., Hanson, P. C., and Read, J. S.: LakeMetabolizer: An R package for estimating lake metabolism from free-water oxygen using diverse statistical models, Inland Waters, 6, 622–636, https://doi.org/10.1080/iw-6.4.883, 2016.

Wu, G. and Liu, Y.: Seasonal water exchanges between China's Poyang Lake and its saucer-shaped depressions on river deltas, Water, 9, 884, https://doi.org/10.3390/w9110884, 2017.

Wu, H., Hao, B., Jo, H., and Cai, Y.: Seasonality and species specificity of submerged macrophyte biomass in shallow lakes under the influence of climate warming and eutrophication, Front. Plant Sci., 12, 678259, https://doi.org/10.3389/fpls.2021.678259, 2021.

Wu, T., Qin, B., Brookes, J. D., Shi, K., Zhu, G., Zhu, M., Yan, W., and Wang, Z.: The influence of changes in wind patterns on the areal extension of surface cyanobacterial blooms in a large shallow lake in China, Sci. Total Environ., 518–519, 24–30, https://doi.org/10.1016/j.scitotenv.2015.02.090, 2015.

Xiao, Q., Duan, H., Qin, B., Hu, Z., Zhang, M., Qi, T., and Lee, X.: Eutrophication and temperature drive large variability in carbon dioxide from China's Lake Taihu, Limnol. Oceanogr., 67, 379–391, https://doi.org/10.1002/lno.11998, 2022.

Xiao, Q., Liu, Z., Hu, Z., Wang, W., Zhang, M., Xiao, W., and Duan, H.: Notable changes of carbon dioxide in a eutrophic lake caused by water diversion, J. Hydrol., 603, 127064, https://doi.org/10.1016/j.jhydrol.2021.127064, 2021.

Xiao, Q., Xu, X., Duan, H., Qi, T., Qin, B., Lee, X., Hu, Z., Wang, W., Xiao, W., and Zhang, M.: Eutrophic Lake Taihu as a significant CO_2 source during 2000–2015, Water Res., 170, 115331, https://doi.org/10.1016/j.watres.2019.115331, 2020.

Xiao, W., Liu, S., Wang, W., Yang, D., Xu, J., Cao, C., Li, H., and Lee, X.: Transfer coefficients of momentum, heat and water vapour in the atmospheric surface layer of a large freshwater lake, Bound.-Lay. Meteorol., 148, 479–494, https://doi.org/10.1007/s10546-013-9827-9, 2013.

Xing, Y., Xie, P., Yang, H., Wu, A., and Ni, L.: The change of gaseous carbon fluxes following the switch of dominant producers from macrophytes to algae in a shallow subtropical lake of China, Atmos. Environ., 40, 8034–8043, https://doi.org/10.1016/j.atmosenv.2006.05.033, 2006.

https://doi.org/10.5194/egusphere-2026-6709
Preprint. Discussion started: 16 November 2026
© Author(s) 2026. CC BY 4.0 License.

Yin, L., Li, W., Madsen, T. V., Maberly, S. C., and Bowes, G.: Photosynthetic inorganic carbon acquisition in 30 freshwater macrophytes, Aquat. Bot., 140, 48–54, https://doi.org/10.1016/j.aquabot.2016.05.002, 2017.

Zhang, L., Liu, D., Yang, F., Yao, E., Yu, J., Huang, W., Wang, J., and Zhong, J.: Atmospheric CO_2 absorption and counteraction by CH_4 emission across contrasting habitats in a large eutrophic lake, J. Hydrol., 645, 132171, https://doi.org/10.1016/j.jhydrol.2024.132171, 2024.

Zhang, Z., Yu, R., Xia, X., Li, J., Sun, H., Cao, Z., Qi, Z., Lu, C., and Lu, X.: Significant diurnal variation of CO_2 flux from a shallow eutrophic lake: effects of submerged aquatic vegetation and algae bloom, Aquat. Sci., 84, 62, https://doi.org/10.1007/s00027-022-00897-w, 2022.

Zhao, K.: Pattern of Distribution and Change of Aquatic Plant in Taihu Lake, Ph.D. thesis, Nanjing Normal University, Nanjing, China, https://www.cnki.net/KCMS/detail/ (last access: 3 November 2026), 2017 (in Chinese).

Zhu, J., Deng, J., Zhang, Y., Peng, Z., and Hu, W.: Response of submerged aquatic vegetation to water depth in a large shallow lake after an extreme rainfall event, Water, 11, 2412, https://doi.org/10.3390/w11112412, 2019.

Zhu, M., Zhu, G., Nurminen, L., Wu, T., Deng, J., Zhang, Y., Qin, B., and Ventelä, A.-M.: The influence of macrophytes on sediment resuspension and the effect of associated nutrients in a shallow and large lake (Lake Taihu, China), PLoS ONE, 10, e0127915, https://doi.org/10.1371/journal.pone.0127915, 2015.